



# ROS regulated reversible protein phase separation synchronizes plant flowering

Xiaozhen Huang<sup>1,2,6</sup>, Shudong Chen<sup>1,2,3,6</sup>, Weiping Li<sup>4</sup>, Lingli Tang<sup>1,2,3</sup>, Yueqin Zhang<sup>1,2,5</sup>, Ning Yang<sup>1,2</sup>, Yupan Zou<sup>1,2</sup>, Xiawan Zhai<sup>1,2</sup>, Nan Xiao<sup>1,2,3</sup>, Wei Liu<sup>1,2,3</sup>, Pulong Li<sup>4</sup>✉ and Cao Xu<sup>1,2</sup>✉

**How aerobic organisms exploit inevitably generated but potentially dangerous reactive oxygen species (ROS) to benefit normal life is a fundamental biological question. Locally accumulated ROS have been reported to prime stem cell differentiation. However, the underlying molecular mechanism is unclear. Here, we reveal that developmentally produced H<sub>2</sub>O<sub>2</sub> in plant shoot apical meristem (SAM) triggers reversible protein phase separation of TERMINATING FLOWER (TMF), a transcription factor that times flowering transition in the tomato by repressing pre-maturation of SAM. Cysteine residues within TMF sense cellular redox to form disulfide bonds that concatenate multiple TMF molecules and elevate the amount of intrinsically disordered regions to drive phase separation. Oxidation triggered phase separation enables TMF to bind and sequester the promoter of a floral identity gene *ANANTHA* to repress its expression. The reversible transcriptional condensation via redox-regulated phase separation endows aerobic organisms with the flexibility of gene control in dealing with developmental cues.**

Development of multicellular organisms depends on the maintenance and fate decision of a pool of stem cells. In plants, the stem cells are embedded within growing apices known as meristems<sup>1</sup>. The SAM produces all above-ground tissues and shapes overall plant architecture<sup>1,2</sup>. The stem cell fate decision in plant SAM is determined by balancing proliferation of central domain cells for replenishing pools of pluripotent cells with differentiation of periphery cells into lateral organs. This balance is regulated by endogenous and environmental signals. Integration of these signals drives meristems to experience a gradual maturation process accompanied by successive leaf production, called meristem maturation, which often terminates with the meristem differentiating into a flower<sup>2</sup>. The transition to flowering at the proper time achieved by precisely controlled SAM maturation is vital for reproductive success and environmental acclimation of flowering plants.

A program preventing precocious maturation ensures an appropriate duration of vegetative meristem stage for formation of adequate stem cells before activation of floral identity genes. A repression mechanism exerted by an ALOG (*Arabidopsis* LSH1 and *Oryza* G1) family gene *TMF* has recently been described as a such program<sup>3,4</sup>. *TMF* encodes a transcription factor that harbors a DNA-binding domain derived from the XerC/D-like recombinases<sup>3,5</sup>. When *TMF* is mutated, the meristem maturation program is prematurely completed due to a precocious activation of the F-box gene *ANANTHA* (*AN*, a homolog of *Arabidopsis* *UFO*), which forces flower differentiation from a meristem mostly in a vegetative state, leading to early flowering and single-flower primary inflorescence<sup>3,6</sup>. The ALOG family genes in different plant species have been reported to play important roles in nodulation, light signaling, floral organ specification and convergent evolution of lateral organogenesis<sup>7–15</sup>. *TMF* defines a new flowering regulation mechanism independent of the classical florigen pathway<sup>2,3</sup>, but nothing

is known about how it senses and relays cellular or environmental signals to gene expression.

ROS have recently been reported as beneficial signals in regulation of stem cell proliferation and differentiation<sup>16–23</sup>. Histological staining using ROS specific fluorescent dyes showed spatial distribution and functions of different forms of ROS in plant meristems: superoxide accumulates mainly in the central zone of SAM to maintain cell proliferation and hydrogen peroxide enriches primarily in the peripheral zone to promote stem cell differentiation<sup>18,19</sup>. H<sub>2</sub>O<sub>2</sub> directed thiol-based modification of cysteine residues in target proteins represents a chief mechanism of ROS mediated biological effects in redox regulation<sup>24–26</sup>. H<sub>2</sub>O<sub>2</sub> reacts with cysteine residues in proteins to form a sulfenic acid, which can react with a second cysteine in the same or a second protein to form intra- or intermolecular disulfide bonds; in turn, they can be reduced through the action of thiol oxidoreductases, such as the thioredoxins and glutaredoxins<sup>23,24</sup>.

In plant SAM, H<sub>2</sub>O<sub>2</sub> is highly reactive with tightly restricted cellular level and spatial localization, which requires its signal sensing and transmitting to be finely controlled in a relatively undisturbed micro-environment. One way to achieve such precise spatiotemporal control of a complicated biochemical process is to regulate the localization of reaction components<sup>27,28</sup>. Biomolecular condensates, micrometer-scale membraneless compartments formed by liquid–liquid phase separation, can concentrate and confine proteins and nucleic acids to prevent the biochemical reactions from outside perturbation<sup>27</sup>. Protein phase separation has recently been found to implicate in acclimation responses to cellular pH levels, heat and oxidative stress in yeast and animals<sup>29–34</sup>. While phase separation-involved stem cell regulation begins to emerge in animals<sup>35</sup>, nothing is known about how cellular or environmental signals trigger/induce protein phase separation to regulate plant stem

<sup>1</sup>State Key Laboratory of Plant Genomics, National Center for Plant Gene Research (Beijing), Institute of Genetics and Developmental Biology, The Innovative Academy of Seed Design, Chinese Academy of Sciences, Beijing, China. <sup>2</sup>CAS-JIC Centre of Excellence for Plant and Microbial Science, Institute of Genetics and Developmental Biology, Chinese Academy of Sciences, Beijing, China. <sup>3</sup>University of Chinese Academy of Sciences, Beijing, China.

<sup>4</sup>Beijing Advanced Innovation Center for Structural Biology, Beijing Frontier Research Center for Biological Structure, Tsinghua-Peking Joint Center for Life Sciences, School of Life Sciences, Tsinghua University, Beijing, China. <sup>5</sup>College of Coastal Agricultural Sciences, Guangdong Ocean University, Zhanjiang, China. <sup>6</sup>These authors contributed equally: Xiaozhen Huang, Shudong Chen. ✉e-mail: [pilongli@mail.tsinghua.edu.cn](mailto:pilongli@mail.tsinghua.edu.cn); [caoxu@genetics.ac.cn](mailto:caoxu@genetics.ac.cn)

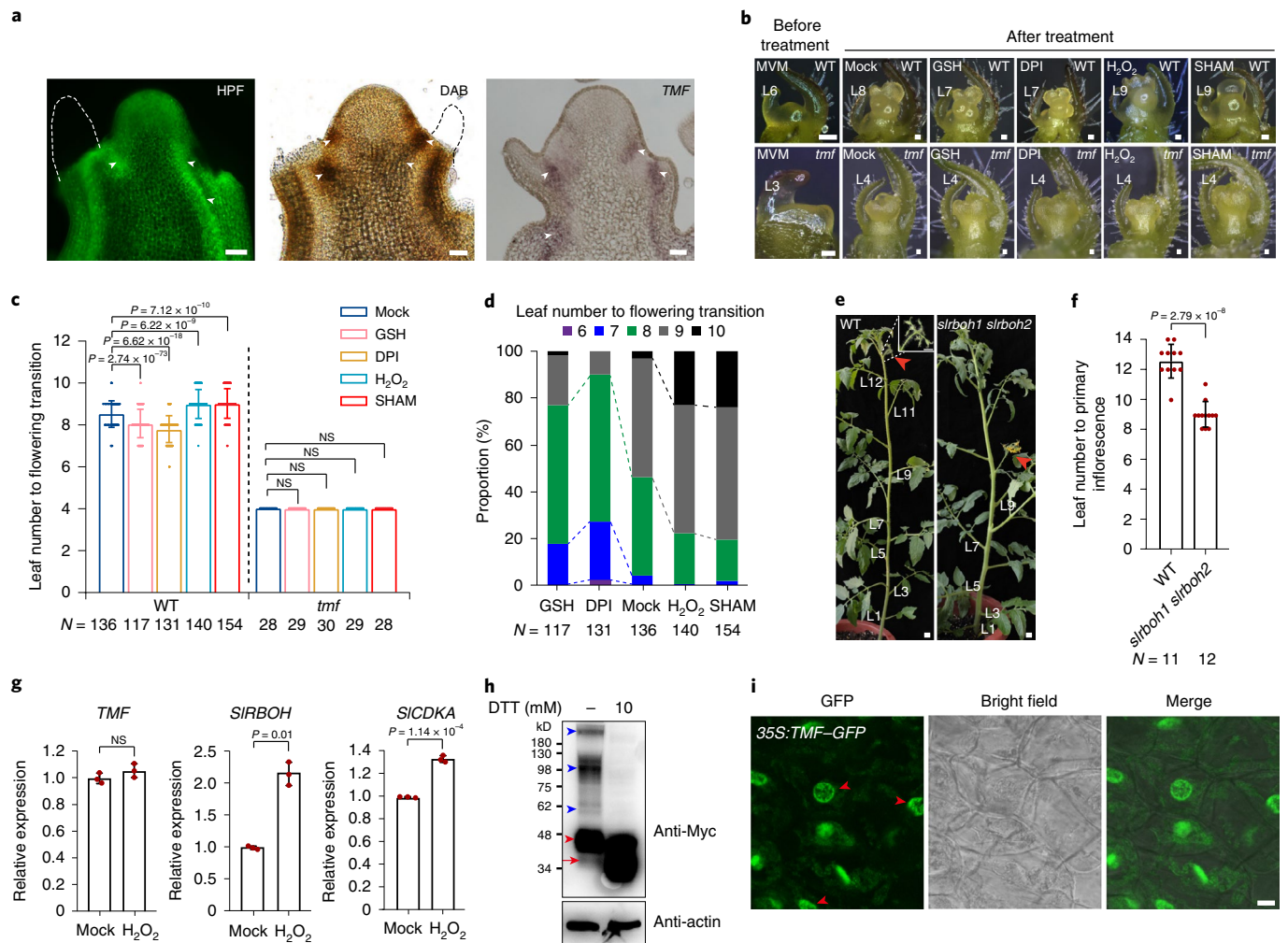


**Fig. 1 | H<sub>2</sub>O<sub>2</sub> represses flowering transition through TMF.** **a**, Spatial distribution of H<sub>2</sub>O<sub>2</sub> and TMF transcripts indicated by HPF staining (left), DAB staining (middle) and in situ hybridization (right) in tomato SAMs, respectively. Scale bar, 50  $\mu$ m. Each experiment was conducted three times with similar results. **b,c**, Stereoscope images (**b**) and quantitative data (**c**) comparing flowering transition indicated by leaf production until the floral meristem stage transition among mock and GSH (1 mM), DPI (0.5  $\mu$ M), H<sub>2</sub>O<sub>2</sub> (10 mM), SHAM (50  $\mu$ M) treated wild type (WT) (upper) and *tmf* (bottom). Leaf production is indicated by leaf number. L, leaf; NS, not significant. Scale bar, 50  $\mu$ m. Sample size of each reagent treatment for the WT and *tmf* mutant is 136, 117, 131, 140, 154, 28, 29, 30, 29 and 28, respectively. **d**, Distribution of leaf production until floral meristem transition in 678 tomato plants under various redox chemical treatments. **e,f**, Representative images (**e**) and quantification data (**f**) showing the early flowering phenotypes of *slrboh1 slrboh2* mutant plants. Red arrow head indicates inflorescences. Scale bar, 1.8 cm. **g**, RT-qPCR showing the expression of TMF, SIRBOH and SICDKA in SAM treated with or without H<sub>2</sub>O<sub>2</sub> (10 mM) for 36 h ( $n=3$ ). **h**, Western blot analysis of TMF proteins. Actin serves as a loading control. Blue and red arrow heads and the red arrow indicate oligomers, dimers and monomers, respectively. Each experiment was conducted three times with similar results. **i**, Confocal microscopy images showing TMF-GFP condensates formed in nuclei in the meristem of 35S:TMF-GFP transgenic tomato plants. Scale bars, 7.5  $\mu$ m. Three independent assays with similar results were conducted.

cell activity. Here we uncover a new protein phase separation mechanism achieved by ROS provoked disulfide bonding and DNA binding of a transcription factor, by which plants exploit developmentally produced ROS to direct stem cell fate for flowering transition.

## Results

**ROS regulates flowering transition through TMF.** To explore the role of ROS in plant flowering transition, we stained the transition meristem stage toward floral transition of tomato SAMs with fluorescent H<sub>2</sub>O<sub>2</sub> probe hydroxyphenyl fluorescein (HPF)<sup>36</sup> and observed intense signals of H<sub>2</sub>O<sub>2</sub> in peripheral zones and initiating vasculature cells (Fig. 1a, left). This pattern was confirmed by staining using nonfluorescent H<sub>2</sub>O<sub>2</sub> dye 3,3'-diaminobenzidine (DAB)<sup>18</sup> (Fig. 1a, middle). The distribution of H<sub>2</sub>O<sub>2</sub> in tomato SAM

reminisces the spatial expression of TMF we reported previously<sup>3,4</sup>. TMF expresses at the periphery of the transition meristem in boundary regions, and into initiating vasculature cells (Fig. 1a, right), matching the pattern of H<sub>2</sub>O<sub>2</sub>.

Recalling the known role of TMF in preventing pre-maturation of meristem, we hypothesized that local enrichment of H<sub>2</sub>O<sub>2</sub> may regulate meristem maturation through TMF. To address this, we manipulated endogenous H<sub>2</sub>O<sub>2</sub> levels in tomato seedlings by exogenously applying H<sub>2</sub>O<sub>2</sub> and related chemicals and investigated their effects on floral transition, which is reflected by the number of leaf primordium produced before vegetative meristems transitioning into floral meristems<sup>37</sup>. The DAB and HPF staining confirmed that application of these chemicals can alter H<sub>2</sub>O<sub>2</sub> levels in the SAM (Extended Data Fig. 1a–c). Treatments using exogenous

H<sub>2</sub>O<sub>2</sub> or peroxidase inhibitor salicylhydroxamic acid (SHAM)<sup>36</sup> that elevates endogenous H<sub>2</sub>O<sub>2</sub> levels delayed the floral transition (Fig. 1b,c). In contrast, application of glutathione (GSH) or oxidase inhibitor diphenylene iodonium (DPI) that decreases cellular H<sub>2</sub>O<sub>2</sub> level<sup>38</sup> promoted flowering earlier by one leaf than untreated plants (Fig. 1b,c). However, the flowering transition of *tmf* null mutant is not affected by the same treatments. This was confirmed in a weaker *TMF* mutant allele *tmf-2* (refs. <sup>3,4</sup>), whose floral transition similarly shows less sensitivity to H<sub>2</sub>O<sub>2</sub> level changes (Extended Data Fig. 1d,e).

Analysis of flowering transition in all treated plants (sample size 678 plants) showed that oxidative chemicals dramatically increased the proportion of late-flowering plants that produce nine to ten leaves before floral transition, but reducing cellular H<sub>2</sub>O<sub>2</sub> level significantly increased the proportion of early flowering plants that flower after six to seven leaves (Fig. 1d). These results suggested that exogenous application of H<sub>2</sub>O<sub>2</sub> alters flowering transition by regulating meristem maturation. To investigate how endogenous H<sub>2</sub>O<sub>2</sub> affects tomato flowering transition, we used CRISPR-Cas9 technology to create null mutants of *respiratory burst oxidase homolog* (*RBOH*), the nicotinamide adenine dinucleotide phosphate oxidase that produces H<sub>2</sub>O<sub>2</sub> in plants. Two *RBOH* members (*SIRBOH1* and *SIRBOH2*) that highly express in SAMs were selected for gene editing (Extended Data Fig. 1f,g). We designed two guide RNAs for each gene and assembled all four gRNAs into one construct to create double knock-out mutants (Extended Data Fig. 1h). The endogenous H<sub>2</sub>O<sub>2</sub> level indeed decreased in *slrboh1 slrboh2* mutant (Extended Data Fig. 1i). The *slrboh1 slrboh2* seedlings showed accelerated meristem maturation toward flowering transition (Extended Data Fig. 1j). The mature *slrboh1 slrboh2* plants flower about three leaves earlier than the wild type (Fig. 1e,f). Together, these results demonstrate that H<sub>2</sub>O<sub>2</sub> serves as a developmental signal to regulate flowering transition through *TMF*.

To explore the underlying molecular mechanism, we examined if *TMF* transcriptionally responds to H<sub>2</sub>O<sub>2</sub>. Quantitative real-time PCR (RT-qPCR) analyses showed that H<sub>2</sub>O<sub>2</sub> treatment does not induce significant transcriptional changes of *TMF* compared to previously reported H<sub>2</sub>O<sub>2</sub> responsive genes<sup>39,40</sup> (Fig. 1g). We then investigated whether *TMF* protein responds to H<sub>2</sub>O<sub>2</sub> and related redox regulations. Given that *TMF* predominantly expresses in vegetative meristems, we generated *35S:TMF-Myc* transgenic lines in the *falsiflora* (*fa*) mutant, a classic tomato mutant overproliferates vegetative meristems<sup>6</sup>. The immunoblotting analysis against *TMF-Myc* proteins showed larger aggregated bands, indicating possible presence of oligomers and dimers (Fig. 1h). Adding dithiothreitol (DTT) shifted the pattern, showing a dramatic decrease of oligomers and dimers, but increase of monomers (Fig. 1h). These results suggest that *TMF* protein behavior is regulated by redox state. To explore *TMF* protein behavior in living cells, we took advantage of a previously identified green fluorescent protein-*TMF* (*GFP-TMF*) transgenic line in which the fusion protein rescues all *tmf* mutant phenotypes<sup>3</sup>. Confocal microscopy imaging showed *TMF-GFP* puncta in the nuclei (Fig. 1i), reminiscent of biomolecular condensates formed by protein liquid-liquid phase separation<sup>27,28</sup>. The punctate localization and redox-regulated oligomerization of *TMF* suggests the potential of protein phase separation.

**H<sub>2</sub>O<sub>2</sub> promotes *TMF* phase separation.** Phase separation often occurs in proteins that have intrinsically disordered regions (IDRs) and the capability for multivalent interactions<sup>27,41</sup>. *TMF* harbors one typical IDR at the N terminus (IDR1) and one short IDR at the C terminus (IDR2) (Fig. 2a and Extended Data Fig. 2a). While purifying recombinantly expressed *TMF* proteins, we observed that cooling on ice made the sample solutions turbid and the solution became clear on raising the temperature to room temperature (Fig. 2b). Microscopy observation of the turbid solution revealed

droplets of various sizes, indicating coexistence of a dense and a dilute phase (Fig. 2c).

To facilitate the observation, we purified recombinantly expressed *GFP-TMF* fusion proteins, which formed spherical droplets with an aspect ratio (maximal diameter to minimal diameter) close to one (Fig. 2d and Extended Data Fig. 2b), indicating a high degree of circularity. We then performed *in vitro* phase separation assays to generate a phase diagram by systematically changing *TMF* protein and salt concentrations to assess the conditions that promote condensate formation. Under these conditions, we observed a continuum of phases from barely detectable small foci to regular droplets and large droplet clusters (Fig. 2e). The *GFP-TMF* proteins started to form visible spherical droplets at a concentration of 1 μM in a buffer with 100 mM NaCl. The droplet abundance increases with the decrease of salt concentration when the protein concentration is constant. It also increases as protein concentration increases with constant salt concentration, indicating that it is sensitive to salt and protein concentrations (Fig. 2e). Using time-lapse microscopy, we found that *TMF* droplets can fuse by necking and relaxation into a spherical shape on intersection of two droplets (Fig. 2f and Supplementary Video 1), suggesting their dynamic property. This was validated by fluorescence recovery after photobleaching (FRAP) analysis, in which we bleached the centers of large droplets and monitored recovery. Around 30% of the originally detected signal intensity of the *GFP-TMF* droplets recovered within 16 min after photobleaching (Fig. 2g,h and Supplementary Video 2).

To investigate phase separation properties of *TMF* *in vivo*, we expressed *TMF-GFP* fusion proteins in tomato protoplasts. *TMF* proteins showed the punctate localization in nuclei, colocalizing with Hoechst-stained chromatin (Fig. 2i). Approximately 50% of transfected cells exhibited this punctate pattern for *TMF* signal (Extended Data Fig. 2c), indicating formation of biomolecular condensates. FRAP analysis showed that approximately 70% of the bleached *TMF* condensates were again visible within 30 s (Extended Data Fig. 2d,e and Supplementary Video 3), suggesting that *TMF* dynamically exchange and form into nuclei condensates. This was confirmed by FRAP analysis in living plants. The bleached condensates in nucleus of *GFP-TMF* transgenic plants could recover within 30 s after bleaching (Fig. 2j,k and Supplementary Video 4), indicating the rapid exchange kinetics of *TMF* condensates in planta. It is noted that the FRAP recovery time of *TMF* condensates in living cells is much shorter than droplets formed *in vitro*. The difference is reminiscent of the fact that phase separation driven by low-complexity regions often undergoes further solidification in test tubes<sup>42,43</sup>. Alternatively, it might be explained by the lack of additional charged interactors, such as nucleic acids, which improve the dynamic of condensates in *in vitro* purified proteins. Collectively, these results suggest that *TMF* undergoes phase separation *in vitro* and form condensates *in vivo*.

We then determined whether the phase separation of *TMF* is sensitive to oxidant/reductant environment. We held the *GFP-TMF* protein and salt concentrations constant but varied the concentrations of H<sub>2</sub>O<sub>2</sub> and reducing reagent DTT. The addition of a relatively low concentration (1 mM) of H<sub>2</sub>O<sub>2</sub> led to an enhancement in droplet formation, markedly fewer droplets were formed as the concentration reaches higher than 10 mM (Fig. 2l and Extended Data Fig. 3a). Notably, the presence of any tested concentration of DTT dramatically disrupted droplet formation (Fig. 2l and Extended Data Fig. 3a). This effect was confirmed using another reducing reagent Tris (2-carboxyethyl) phosphine hydrochloride (Extended Data Fig. 3b,c). Moreover, we observed the apparent chemical rescue of *TMF*'s droplet formation in samples containing both DTT and H<sub>2</sub>O<sub>2</sub> (Fig. 2l and Extended Data Fig. 3a), indicating that phase separation capacity of *TMF* is reversible and can be controlled via an oxidation-reduction switch. To quantitatively investigate the redox-regulated phase separation of *TMF* protein, we performed

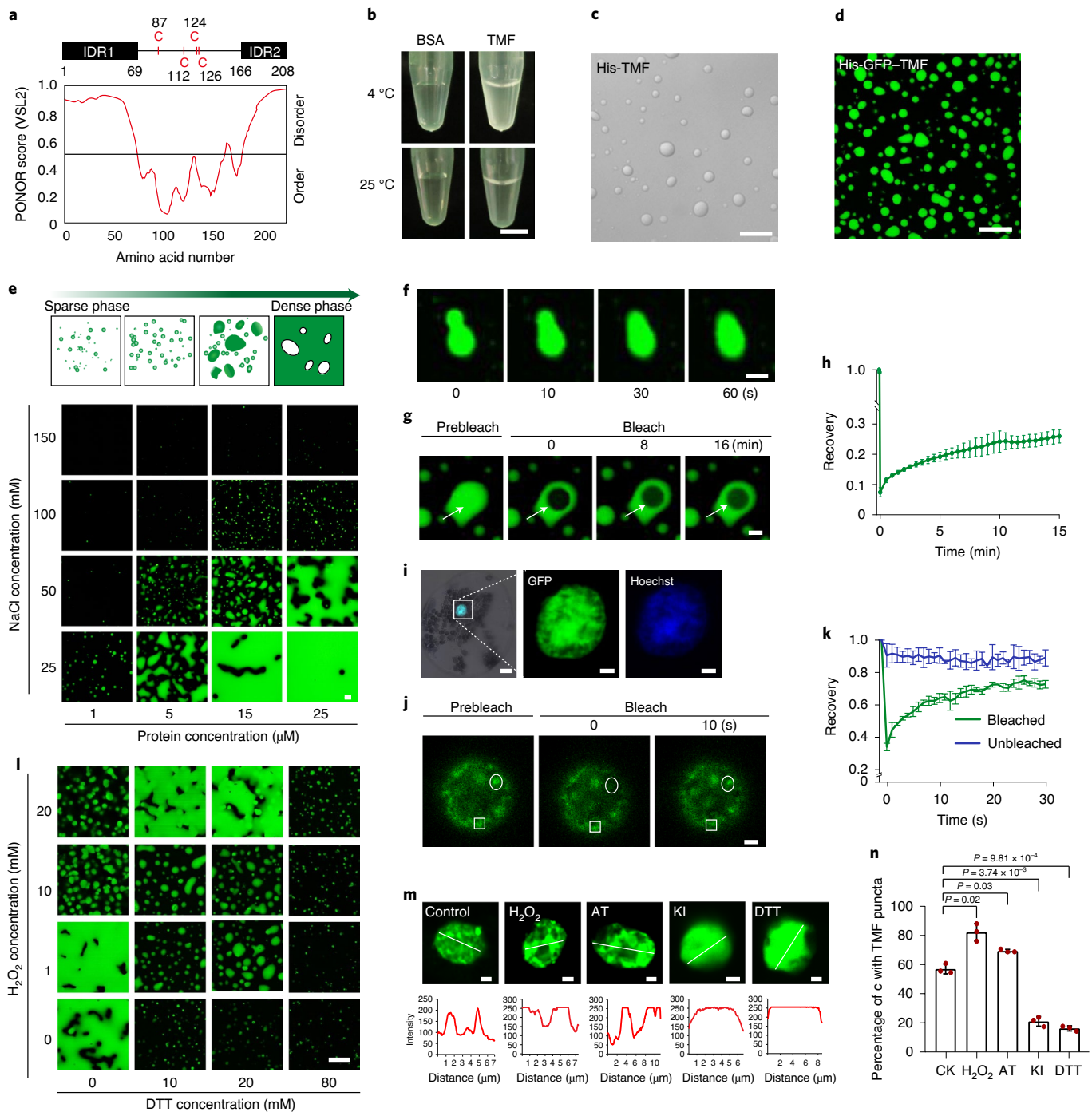


**Fig. 2 | TMF undergoes phase separation in vitro and in vivo.** **a**, IDRs and cysteine residues in TMF proteins. **b**, Visualization of turbid solution of His-TMF proteins. Bovine serum albumin serves as a control. Scale bar, 3.5 mm. **c,d**, Representative differential interference contrast and fluorescence image showing the droplets formed by His-TMF (**c**) and His-GFP-TMF (**d**) proteins. Scale bar, 10  $\mu$ m. Three independent assays with similar results were carried out. **e**, Phase diagram of GFP-TMF droplets. Scale bar, 5  $\mu$ m. Three independent assays with similar results were carried out. **f**, Time-lapse microscopy showing fusion dynamics of GFP-TMF droplets. Images are representative of five independent fusion events. Time 0 indicates the time of start recording. Scale bar, 1  $\mu$ m. **g**, FRAP assay showing dynamic property of GFP-TMF droplets. Time 0 indicates the time of the photobleaching pulse. White arrows show the bleached area in droplets. Scale bar, 1  $\mu$ m. **h**, Quantification data of FRAP assays for GFP-TMF droplets. Data are representative of four independent FRAP events. **i**, Condensates formed by TMF-GFP fusion proteins (green) in the nuclei stained by Hoechst (blue) of tomato protoplast cells. Scale bar, 2  $\mu$ m. Three independent assays with similar results were carried out. **j,k**, Images (**j**) and quantitative FRAP data (**k**) showing the dynamic property of TMF-GFP condensates in *35S:TMF-GFP* transgenic plants. The bleached (green line) event occurs at a time of 0 s. The unbleached (blue line) was used as control. Quantitative data are representative of three independent photobleaching events. Scale bar, 2  $\mu$ m. **l**, Phase diagram showing droplet formation of GFP-TMF protein under various concentration combinations of  $H_2O_2$  and DTT with constant protein concentration (25  $\mu$ M). Scale bar, 5  $\mu$ m. Three independent assays with similar results were performed. **m,n**, Imaging (**m**) and quantification (**n**) indicating effects of various redox chemicals on TMF-GFP condensate formation in tomato protoplasts. Scale bar, 2  $\mu$ m. Protein concentrations were 15  $\mu$ M in **c,d** and 25  $\mu$ M in **f,g**; NaCl concentrations were 25 mM in **c,d,f,g**. Data are presented as means ( $\pm$ s.d.) ( $n = 63, 73, 49, 67, 55$ ; two-tailed  $t$ -test) in **n**.

a sedimentation assay to separate the condensed liquid phase and the aqueous phase by centrifugation (Extended Data Fig. 3d). We found that adding DTT reduced the proportion of TMF present in the condensate phase (pellet), while  $H_2O_2$  promoted the formation of the condensate phase (Extended Data Fig. 3e,f), confirming the redox responsive property of TMF condensates.

Extending these insights from *in vitro* experiments into plant cells, we treated tomato protoplasts with a variety of redox chemicals and quantified the percentage of the cells showing TMF condensates. Consistent with the trends we observed in the *in vitro* phase separation assays, exogenous  $H_2O_2$  increased condensation of TMF–GFP in nuclei, while DTT significantly disrupted this process (Fig. 2m,n). Moreover, treatment of protoplasts with a general  $H_2O_2$  scavenger, potassium iodide (KI)<sup>19</sup>, diminished phase separation, while it can be dramatically improved on elevating overall  $H_2O_2$  concentration via application of catalase inhibitor amino-1,2,4-triazole<sup>44</sup> (Fig. 2m,n). These results indicate that  $H_2O_2$  and related redox state regulate phase separation of TMF protein.

**Cysteine oxidation enables phase separation of TMF.** We next explore the driving forces of TMF phase separation. Phase-separating IDRs often encompass low-complexity regions enriched with polar amino acid residues such as glutamine and asparagine<sup>27</sup>. The IDR1 region of TMF contains high asparagine content (Extended Data Fig. 2a). We mutated the eight asparagine residues in IDR1 into alanines (TMF<sup>Idr1</sup>) and deleted the shorter IDR2 region (TMF<sup>Δidr2</sup>), respectively (Extended Data Fig. 3g). Both recombinantly expressed TMF<sup>Idr1</sup> and TMF<sup>Δidr2</sup> showed weaker droplet formation capacity than normal TMF (Fig. 3a and Supplementary Fig. 1). Expression of GFP fusion proteins of TMF<sup>Idr1</sup> and TMF<sup>Δidr2</sup> in tomato protoplasts showed dramatic decreases in condensate formation (Fig. 3b,c and Extended Data Fig. 3h). These observations indicated that phase separation of TMF is, in part, driven by IDRs.

Four cysteine residues in the folded region between the two IDRs draw our attention since cysteine residues within proteins are typical targets for  $H_2O_2$  mediated oxidation. We mutated four cysteines individually into serines to generate TMF<sup>C87S</sup>, TMF<sup>C112S</sup>, TMF<sup>C124S</sup> and TMF<sup>C126S</sup> protein variants (Extended Data Fig. 3g and Supplementary Fig. 1). *In vitro* phase separation assays indicated that mutations of cysteines diminished TMF's capacity of phase separation in varying degrees (Fig. 3a). In contrast to a slight decrease of droplet formation of TMF<sup>C87S</sup>, TMF<sup>C112S</sup> and TMF<sup>C126S</sup> can only form scattered aggregates with irregular shapes. TMF<sup>C124S</sup> almost completely eliminated the phase separation capacity (Fig. 3a and Extended Data Fig. 3g). These results were confirmed by condensate assessments of GFP fusion proteins in tomato protoplasts in which the TMF<sup>C124S</sup> variant showed the most pronounced loss of biological condensate (Fig. 3b,c). We also noted that there was no GFP fluorescence signal detected for the TMF<sup>C126S</sup> variant in protoplasts, possibly due to low protein stability (Extended Data Fig. 3i). Together, *in vitro* and *in vivo* results suggest that both IDRs and cysteine residues are required for TMF phase separation.

The most common reversible oxidative modification of a protein is the formation of disulfide bonds through oxidation of cysteine residues<sup>24</sup>. We analyzed recombinantly expressed TMF proteins by mass spectrometry and found that C124 indeed forms intramolecular disulfide bonds with C126. Intermolecular disulfide bonds also form via crosslinking C112–C124 and C112–C126 (Fig. 3d and Extended Data Fig. 4a). To test the causal link between proper disulfide bonds formation and TMF phase separation, we used protein-disulfide isomerase (PDI) to manipulate disulfide bond arrangement. PDI can catalyze thiol-disulfide interchange (oxidation/reduction) and disulfide bond rearrangement (isomerization) in substrate proteins, depending on redox states of its active sites<sup>45</sup> (Extended Data Fig. 4b). We incubated PDI with TMF protein in a

redox balancing buffer (1 mM GSH + 0.2 mM glutathione disulfide (GSSG), GSH/GSSG = 5) that allows disulfide formation (oxidation) while maintaining sufficient reducing power to break incorrect disulfides<sup>46</sup>. The treatment did not significantly change TMF phase separation behavior (Fig. 3e,f). Mass spectrometry analysis confirmed that oxidative PDI did not isomerize existed disulfide bonds (Extended Data Fig. 4c), suggesting the stability of existing disulfide bonds in TMF. To further test PDI's function in catalyzing disulfide bond formation and its effects on TMF phase separation, we reduced TMF protein thoroughly with a 4-h treatment with 100 mM DTT. After dialysis removal of DTT, we found that the reduced TMF lost phase separation capacity and it failed to recover after a long time of exposure in air (Fig. 3g,h). Notably, PDI can catalyze the disulfide bond reformation of reduced TMF protein and thus largely rescue its phase separation (Fig. 3g,h), demonstrating that phase separation of TMF relies on disulfide bonds formed by cysteine oxidation. Therefore, cysteines within TMF sense redox conditions to form intermolecular disulfide bonds that concatenate TMF molecules to enhance IDR-driven phase separation.

**TMF transcriptional condensates repress AN expression.** Given the fact that TMF is a putative transcription factor that represses flowering transition, we hypothesize that  $H_2O_2$  signaling can be perceived by cysteine residues in TMF, which triggers phase separation of TMF to regulate transcription of flowering genes. Previous studies have shown that TMF synchronizes tomato flowering by preventing precocious activation of AN, and the *an* mutant is completely epistatic to *tmf*<sup>f</sup>. We therefore tested whether AN is a direct downstream target gene of TMF. The yeast one-hybrid assay showed that TMF physically interacted with AN promoter (Fig. 4a and Extended Data Fig. 5a–d). To confirm the direct binding *in vivo*, we performed chromatin immunoprecipitation (ChIP) analysis in planta by using the vegetative meristem tissue collected from 35S:TMF–Myc transgenic plants. The ChIP–qPCR assays showed appreciable enrichment of TMF–Myc protein in the promoter regions of AN (Fig. 4b and Extended Data Fig. 5e). This direct binding was further validated by the electrophoretic mobility shift assay (EMSA) using recombinantly expressed TMF protein (Fig. 4c). These results indicate that AN is a direct target of TMF. Notably, cysteine residue and IDR mutations of TMF comprised the promoter binding ability, shown by yeast one-hybrid and EMSA assays (Fig. 4c and Extended Data Fig. 5b–d), suggesting that phase separation is essential for TMF's transcriptional binding capability.

We next assessed the phase separation property of TMF as it interacts with target DNA sequences. When 5'-fluorophore labeled DNA fragments from the AN promoter were incubated with recombinantly expressed GFP–TMF protein, phase-separated droplets formed in a 150 mM NaCl solution (a physiologically relevant salt concentration) (Fig. 4d), few droplets formed in samples with the same TMF protein concentration but lacking DNA (Fig. 2e). A phase diagram assay confirmed that the presence of these DNA molecules promoted TMF's phase separation (Fig. 4d). Supporting this, FRAP analysis showed that TMF–DNA complex droplets have significantly improved recovery after photobleaching compared to DNA-free protein droplets (Fig. 4e,f, Supplementary Video 5 and Fig. 2g,h). We then incubated TMF–DNA complexes in variable redox conditions created by combinations of different DTT and  $H_2O_2$  concentrations (Fig. 4g and Extended Data Fig. 6a). DTT dramatically disrupted phase separation at all tested concentrations, while  $H_2O_2$  promoted droplet formation at low concentrations (Fig. 4g and Extended Data Fig. 6a).  $H_2O_2$  rescued the disrupting effects of DTT (Fig. 4g and Extended Data Fig. 6a), confirming that increasing  $H_2O_2$  oxidant concentration can counterbalance the disulfide bond disruption by DTT to promote droplet formation. This redox responsive property of TMF–DNA droplets is validated by the sedimentation assay (Extended Data Fig. 6b,c).

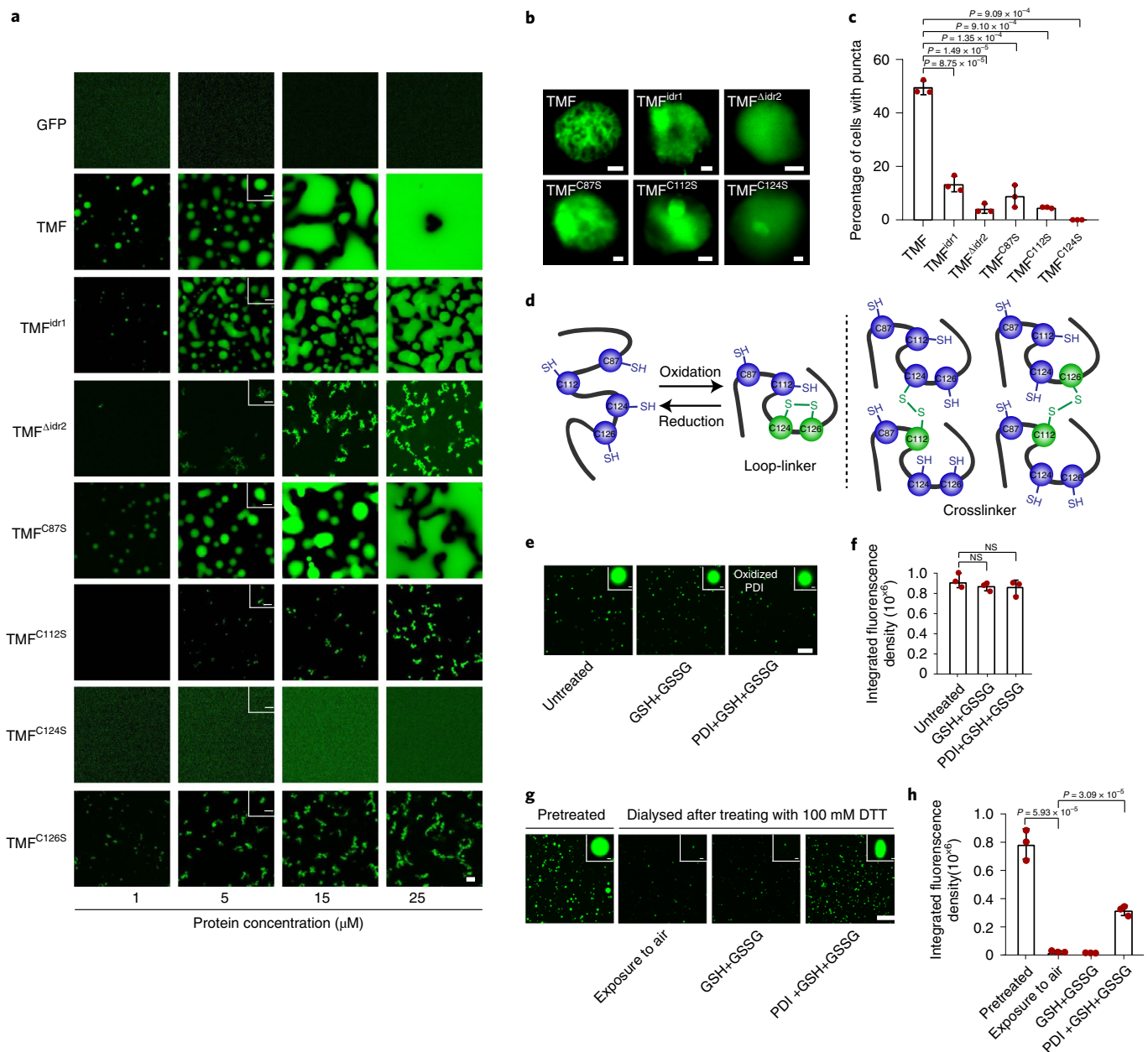


**Fig. 3 | Redox-regulated disulfide bonding determines phase status of TMF.** **a**, Phase-separated droplets formed by TMF variants with IDR or cysteine mutations. Representative confocal images showing droplet formation of each mutated TMF protein (right). Insets indicate the shape of individual droplet. NaCl concentration, 25 mM; scale bars, 5 μm (large picture), 2 μm (insets). Three independent assays with similar results were performed. **b**, Subcellular localization pattern of TMF variants with IDR or cysteine mutations in nuclei of transfected tomato protoplasts. Scale bars, 2 μm. **c**, Percentage of transfected tomato protoplast cells showing nuclei condensates from TMF and its mutant variants ( $n = 69, 52, 94, 67, 65, 69$ ). **d**, Schematics illustrating the intermolecular and intramolecular disulfide bonds identified by LC-MS/MS from recombinantly expressed TMF protein. C, cysteine residue; red line, loop-link and crosslink forms of disulfide bonds. **e–h** Representative confocal microscopy images and quantitative data showing the effects of PDI treatments on droplet formation of normal (**e,f**) and reduced (**g,h**) GFP-TMF proteins. Protein concentrations, 8 μM (**e**) and 5 μM (**g**); salt concentration, 25 mM; scale bars, 50 μm (**e**), 25 μm (**g**) and 1 μm (inset). Three technical replicates of data are presented ( $n = 3$ ). In **c,f,h**, data are presented as means ( $\pm$ s.d.) (two-tailed *t*-test).

To explore how ROS related redox regulation of TMF's phase separation affects *AN* transcription, we conducted a series of transcriptional activity assays using the beta-glucuronidase (GUS)–luciferase (LUC) dual reporter system in tobacco leaves (Fig. 5a). The results showed that TMF repressed *AN* transcription (Fig. 5b). Exogenous application of H<sub>2</sub>O<sub>2</sub> or amino-1,2,4-triazole and SHAM that increase cellular H<sub>2</sub>O<sub>2</sub> level enhanced the transcriptional repression; however, application of chemicals including KI and DPI attenuated the

transcriptional repression (Fig. 5c). These data indicate that H<sub>2</sub>O<sub>2</sub> is essential for TMF to maintain its transcriptional repression on *AN*. We then examined if floral transition regulated by redox states is *AN* dependent. Given that *AN* is rarely expressed in vegetative and transitional meristems before floral transition due to repression by TMF, H<sub>2</sub>O<sub>2</sub> scavenger treatment that disrupts TMF phase separation would release the repression and result in precocious activation of *AN*. The RT-qPCR analysis using micro-dissected tomato transitional

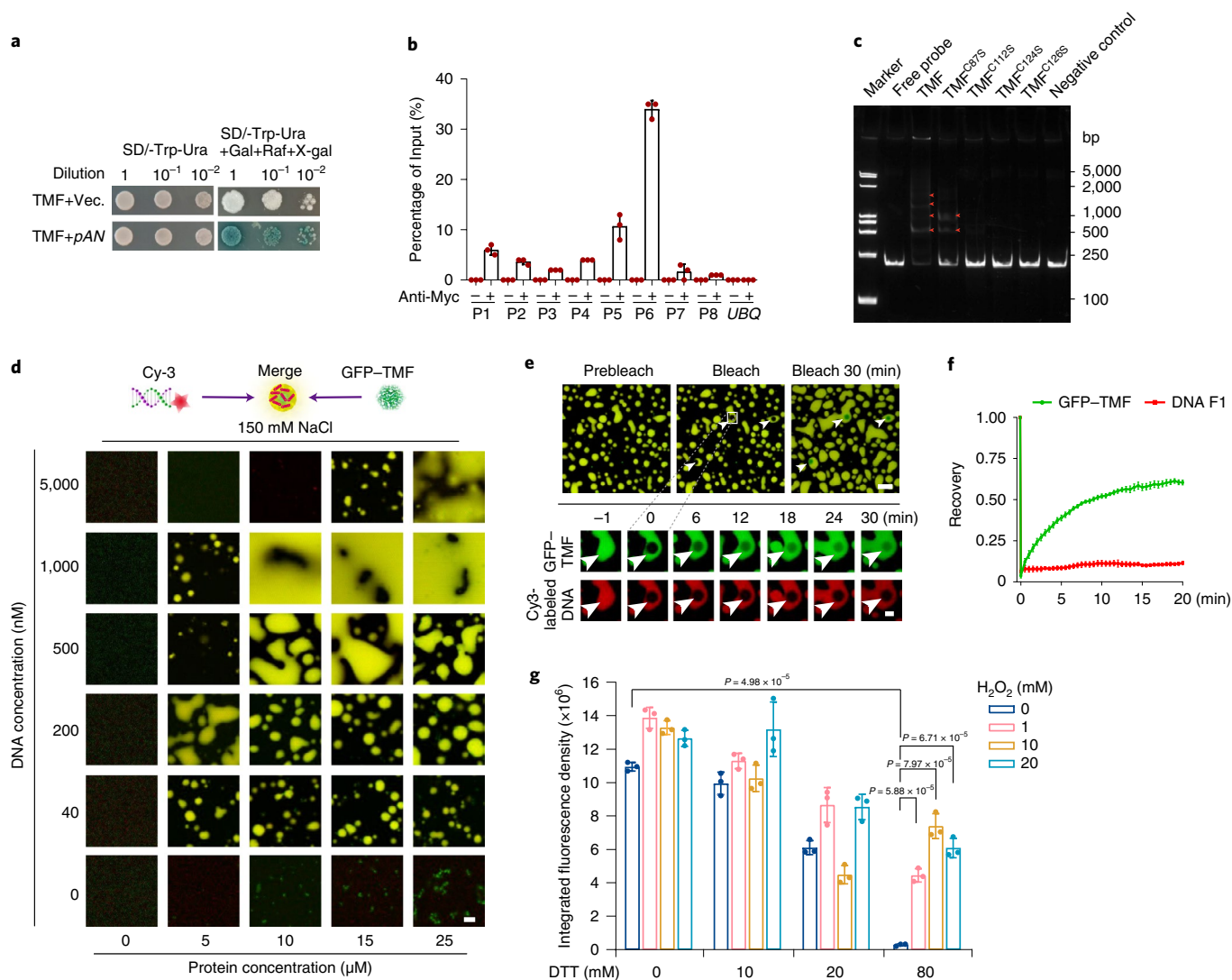


**Fig. 4 | TMF directly targets the *AN* gene.** **a**, Colony growth assessment showing TMF binds to *AN* promoter. **b**, ChIP-RT-qPCR assay indicating that TMF binds to the promoter of *AN* in vivo. Three independent experiments with three technical replicates for each experiment were performed. Data are presented as means ( $\pm$ s.d.) ( $n=3$ ). **c**, EMSA analysis showing DNA-binding properties of TMF and its variants with cysteine mutations. Red arrow head indicates mobility shift of the protein-DNA complex. The DNA fragment of P6 in **b** was used for this assay. Three independent assays were performed. **d**, Phase diagram showing droplet formation of GFP-TMF with Cy-3 labeled DNA fragments from *AN* promoter. Various protein and DNA concentration combinations for this assay as indicated. Green, GFP-TMF; red, Cy-3 labeled DNA F1 (from the  $-1,538$  to the  $-1,667$  bp region upstream from the start codon of *AN*). Merged images (yellow) are shown. Scale bar,  $5\ \mu\text{m}$ . **e, f**, Imaging (**e**) and quantitative data (**f**) from FRAP assay showing dynamic property of biomolecular condensates formed by GFP-TMF and Cy-3 labeled DNA fragments from *AN* promoter. White arrow heads show the bleached area in droplets. Scale bars,  $20\ \mu\text{m}$  (upper panel) and  $1\ \mu\text{m}$  (lower panel). Quantitative data are representative of three independent FRAP events. **g**, Quantification of integrated fluorescence density of the liquid-like droplets formed by GFP-TMF protein with Cy-3 labeled DNA under various concentration combinations of  $\text{H}_2\text{O}_2$  and DTT. Protein concentration,  $15\ \mu\text{M}$ ; DNA concentration,  $500\ \text{nM}$ . Data are presented as means ( $\pm$ s.d.) ( $n=3$ , two-tailed *t*-test).

meristems showed that *AN*'s expression can be precociously activated on DPI treatments in wild-type plants, but not in *tmf* mutants (Fig. 5d). Notably, we also found the precocious upregulation of *AN* in the *slrboh1 slrboh2* double mutant (Fig. 5e). These data explain the early flowering phenotypes of the *slrboh1 slrboh2* double mutant and the plants after reducing chemical and  $\text{H}_2\text{O}_2$  scavenger treatments (Fig. 1b-f). In support of this, previous studies have shown that ectopic expression of *AN* in vegetative meristems leads to precocious adoption of floral identity that promotes early flowering<sup>3</sup>. These results demonstrate that  $\text{H}_2\text{O}_2$  regulated flowering transition relies on TMF regulated expression of *AN*.

Given that cysteine residues within TMF sense developmental ROS, we then explored the functional indispensability of the

cysteine residues in regulating floral transition. The GUS-LUC dual reporter assays indicated that cysteine mutation variants of TMF compromised its transcriptional repression effects on *AN* (Fig. 5f). To validate this in planta, we performed a complementation test by transforming cysteine mutated TMF variant into *tmf* null mutant plants. Compared to the flowering time rescue by normal TMF protein, point mutation of C112, a key cysteine residue for formation of intermolecular disulfide bond, failed to rescue the early flowering defects of *tmf* (Fig. 5g and Extended Data Fig. 6d,e), confirming that TMF's function depends on oxidation triggered disulfide bonding of cysteine residues. Together, these results demonstrate that  $\text{H}_2\text{O}_2$  provoked TMF transcriptional condensates repress *AN* expression to regulate flowering transition.

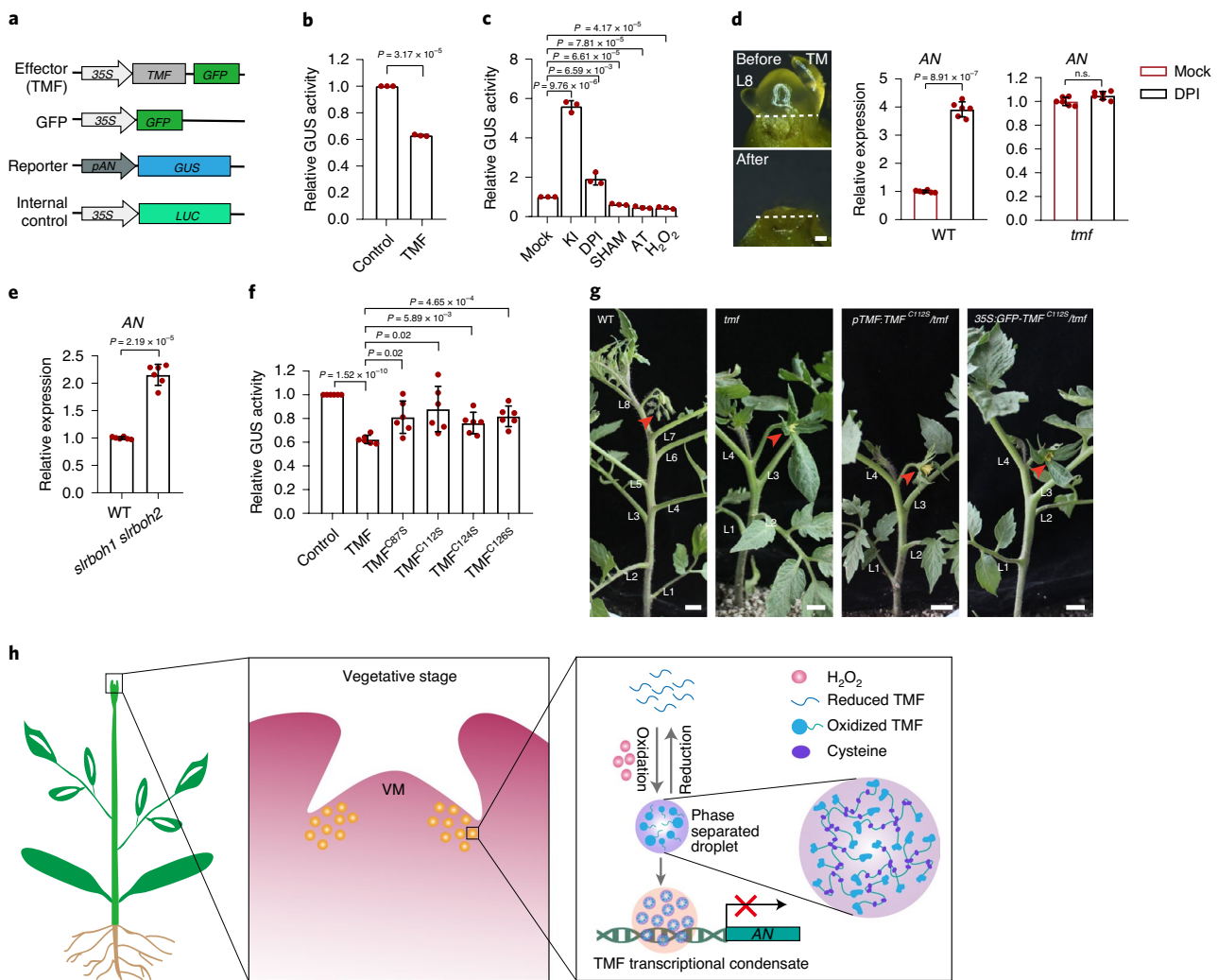


**Fig. 5 |  $H_2O_2$  promoted formation of TMF transcriptional condensates regulate flowering.** **a**, Schematics of the constructs used for dual reporter transcriptional activity assays. **b, c**, Transcriptional repression of AN by TMF (**b**) and the repression affected by redox chemical treatments (**c**). The relative transcriptional activity was indicated by the GUS to LUC ratio. **d**, Micro-dissected transitional meristems (left) from DPI treated plants for RT-qPCR analysis (right). White dashed line indicates the dissection line (left). L, leaf number from first leaf. Scale bar, 100  $\mu$ m. *UBIQUITIN* (*UBI*) served as an internal control, and relative expression was normalized relative to the mock. **e**, RT-qPCR analysis showing the precocious activation of AN in transitional meristems of *slrboh1 slrboh2* mutant. *UBIQUITIN* (*UBI*) served as an internal control, and relative expression was normalized relative to WT. **f**, Cysteine mutated TMF variants comprise its transcriptional repression on AN indicated by relative GUS activity. **g**, Transforming cysteine mutated TMF variant into *tmf* fails to rescue the mutant phenotypes. Red arrows indicate the first inflorescence. Scale bar, 1.8 cm. **h**, The working model of  $H_2O_2$  promoted formation of TMF transcriptional condensates in synchronizing flowering. VM, vegetative meristem. Data of three biological replicates were presented for **b** and **c**, six biological replicates were presented for **f**. Data from two independent experiments with three technical replicates are presented for **d** and **e**. Data are means ( $\pm$  s.d.) ( $n=3$  for **b, c**;  $n=6$  for **d, e, f**, two-tailed *t*-test).

## Discussion

Our findings support a model wherein the spatially distributed  $H_2O_2$  in the boundary region of plant SAM at vegetative stages oxidizes cysteines of TMF protein to form disulfide bonds, which facilitates the IDR-driven phase separation. The phase-separated TMF condensates sequester the AN locus to prevent its precocious activation during meristem maturation to maintain an appropriate duration of vegetative stage for floral transition (Fig. 5h). The SAM lies at the center of plant development, whose activity is strongly influenced by environmental conditions. Flowering is highly plastic under environmental stress, either being accelerated or delayed, aligned to plant developmental stages under stress<sup>47</sup>. As cellular ROS level quickly changes in response to environment conditions, ROS promoted protein phase separation might be an evolved bet-hedging strategy for environmental acclimation of plants.

Biomolecular phase separation is a robust and switch-like behavior happening in numerous biological pathways<sup>27,28</sup>. We discovered that TMF takes advantage of intermolecular disulfide bonds to achieve this switch-like function. TMF contains two IDR regions that mediate phase separation at high protein concentrations and low salt concentrations in vitro. The developmentally produced  $H_2O_2$  promotes the formation of intra- and intermolecular disulfide bonds between highly conserved cysteine residuals of TMF. The intermolecular disulfide bonds enable concatenation of TMF molecules, which enhances phase separation by increasing the valency of IDRs. On the other hand, the intramolecular disulfide bonds cap TMF polymers at finite sizes, which is consistent with its fast dynamics within TMF condensates in vivo. Phase separation of TMF is also strengthened by binding to the promoter of target gene(s). Therefore, the driving force of TMF phase separation includes weak

interactions including multivalent interactions between IDRs, charge-charge interactions between TMF and DNAs, and strong interactions such as intermolecular disulfide bonds. In plant SAM, the oxidative ROS are tightly controlled to maintain the proper cellular level and spatial localization<sup>18,23</sup>. The double-condensation promoting mechanism enables the precise coupling of ROS sensing with loci-specific transcriptional suppression via phase separation. There are about 214,000 cysteine residues encoded in proteins of human genome, about 10–20% of them in cellular cysteine proteome are readily oxidized under aerobic conditions<sup>48</sup>. Our finding that naturally produced ROS promote the formation of transcriptional condensates uncovers a new layer of complexity in redox biology. This mechanism might serve as a common cellular behavior evolved in aerobic organisms for coping with ROS.

### Online content

Any methods, additional references, Nature Research reporting summaries, source data, extended data, supplementary information, acknowledgements, peer review information; details of author contributions and competing interests; and statements of data and code availability are available at <https://doi.org/10.1038/s41589-021-00739-0>.

Received: 24 August 2020; Accepted: 13 January 2021;

Published online: 25 February 2021

### References

- Irish, V. F. & Sussex, I. M. A fate map of the *Arabidopsis* embryonic shoot apical meristem. *Development* **115**, 745–753 (1992).
- Park, S. J., Eshed, Y. & Lippman, Z. B. Meristem maturation and inflorescence architecture—lessons from the Solanaceae. *Curr. Opin. Plant Biol.* **17**, 70–71 (2014).
- MacAlister, C. A. et al. Synchronization of the flowering transition by the tomato *TERMINATING FLOWER* gene. *Nat. Genet.* **44**, 1393–1398 (2012).
- Xu, C., Park, S. J., Van Eck, J. & Lippman, Z. B. Control of inflorescence architecture in tomato by BTB/POZ transcriptional regulators. *Genes Dev.* **30**, 2048–2061 (2016).
- Iyer, L. M. & Aravind, L. ALOG domains: provenance of plant homeotic and developmental regulators from the DNA-binding domain of a novel class of DIRS1-type retrotransposons. *Biol. Direct* **7**, 39 (2012).
- Lippman, Z. B. et al. The making of a compound inflorescence in tomato and related nightshades. *PLoS Biol.* **6**, 2424–2435 (2008).
- Lei, Y., Su, S., He, L., Hu, X. & Luo, D. A member of the ALOG gene family has a novel role in regulating nodulation in *Lotus japonicus*. *J. Integr. Plant Biol.* **61**, 463–477 (2019).
- Takeda, S. et al. CUP-SHAPED COTYLEDON1 transcription factor activates the expression of LSH4 and LSH3, two members of the ALOG gene family, in shoot organ boundary cells. *Plant J.* **66**, 1066–1077 (2011).
- Zhao, L. et al. Overexpression of LSH1, a member of an uncharacterised gene family, causes enhanced light regulation of seedling development. *Plant J.* **37**, 694–706 (2004).
- Yoshida, A., Suzuki, T., Tanaka, W. & Hirano, H.-Y. The homeotic gene long sterile lemma (G1) specifies sterile lemma identity in the rice spikelet. *Proc. Natl Acad. Sci. USA* **106**, 20103–20108 (2009).
- Cho, E. & Zambryski, P. C. ORGAN BOUNDARY1 defines a gene expressed at the junction between the shoot apical meristem and lateral organs. *Proc. Natl Acad. Sci. USA* **108**, 2154–2159 (2011).
- Sato, D.-S., Ohmori, Y., Nagashima, H., Toriba, T. & Hirano, H.-Y. A role for TRIANGULAR HULL1 in fine-tuning spikelet morphogenesis in rice. *Genes Genet. Syst.* **89**, 61–69 (2014).
- Naramoto, S. et al. A conserved regulatory mechanism mediates the convergent evolution of plant shoot lateral organs. *PLoS Biol.* **17**, e3000560 (2019).
- Yoshida, A. et al. TAWAWA1, a regulator of rice inflorescence architecture, functions through the suppression of meristem phase transition. *Proc. Natl Acad. Sci. USA* **110**, 767–772 (2013).
- Chen, F. et al. Genome-wide identification and characterization of the ALOG gene family in *Petunia*. *BMC Plant Biol.* **19**, 600 (2019).
- Owusu-Ansah, E. & Banerjee, U. Reactive oxygen species prime *Drosophila* haematopoietic progenitors for differentiation. *Nature* **461**, 537–541 (2009).
- Morimoto, H. et al. ROS are required for mouse spermatogonial stem cell self-renewal. *Cell Stem Cell.* **12**, 774–786 (2013).
- Zeng, J., Dong, Z., Wu, H., Tian, Z. & Zhao, Z. Redox regulation of plant stem cell fate. *EMBO J.* **36**, 2844–2855 (2017).
- Tsakagoshi, H., Busch, W. & Benfey, P. N. Transcriptional regulation of ROS controls transition from proliferation to differentiation in the root. *Cell* **143**, 606–616 (2010).
- Yang, S. et al. ROS: the fine-tuner of plant stem cell fate. *Trends Plant Sci.* **23**, 850–853 (2018).
- Rampon, C., Volovitch, M., Joliot, A. & Vriza, S. Hydrogen peroxide and redox regulation of developments. *Antioxidants* **7**, 159 (2018).
- Sies, H. & Jones, D. P. Reactive oxygen species (ROS) as pleiotropic physiological signalling agents. *Nat. Rev. Mol. Cell Biol.* **21**, 363–383 (2020).
- Foyer, C. H. & Noctor, G. Redox homeostasis and signaling in a higher-CO<sub>2</sub> world. *Annu. Rev. Plant Biol.* **71**, 157–182 (2020).
- Paulsen, C. E. & Carroll, K. S. Orchestrating redox signaling networks through regulatory cysteine switches. *ACS Chem. Biol.* **5**, 47–62 (2010).
- Poole, L. B. The basics of thiols and cysteines in redox biology and chemistry. *Free Radic. Biol. Med.* **80**, 148–157 (2015).
- Zeida, A. et al. Catalysis of peroxide reduction by fast reacting protein thiols. *Chem. Rev.* **119**, 10829–10855 (2019).
- Banani, S. F., Lee, H. O., Hyman, A. A. & Rosen, M. K. Biomolecular condensates: organizers of cellular biochemistry. *Nat. Rev. Mol. Cell Biol.* **18**, 285–298 (2017).
- Shin, Y. & Brangwynne, C. P. Liquid phase condensation in cell physiology and disease. *Science* **357**, eaaf4382 (2017).
- Kroschwald, S. et al. Different material states of Pub1 condensates define distinct modes of stress adaptation and recovery. *Cell Rep.* **23**, 3327–3339 (2018).
- Franzmann, T. M. et al. Phase separation of a yeast prion protein promotes cellular fitness. *Science* **359**, eaao5654 (2018).
- Riback, J. A. et al. Stress-triggered phase separation is an adaptive, evolutionarily tuned response. *Cell* **168**, 1028–1040.e19 (2017).
- Kato, M. et al. Redox state controls phase separation of the yeast Ataxin-2 protein via reversible oxidation of its methionine-rich low-complexity domain. *Cell* **177**, 711–721.e8 (2019).
- Yang, Y. S. et al. Yeast Ataxin-2 forms an intracellular condensate required for the inhibition of TORC1 signaling during respiratory growth. *Cell* **177**, 697–710.e17 (2019).
- Zhang, G., Wang, Z., Du, Z. & Zhang, H. mTOR regulates phase separation of PGL granules to modulate their autophagic degradation. *Cell* **174**, 1492–1506.e22 (2018).
- Wu, X., Cai, Q., Feng, Z. & Zhang, M. Liquid-liquid phase separation in neuronal development and synaptic signaling. *Dev. Cell* **55**, 18–29 (2020).
- Dunand, C., Crèvecoeur, M. & Penel, C. Distribution of superoxide and hydrogen peroxide in *Arabidopsis* root and their influence on root development: possible interaction with peroxidases. *N. Phytol.* **174**, 332–341 (2007).
- Park, S. J., Jiang, K., Schatz, M. C. & Lippman, Z. B. Rate of meristem maturation determines inflorescence architecture in tomato. *Proc. Natl Acad. Sci. USA* **109**, 639–644 (2012).
- Doussiere, J. & Vignais, P. V. Diphenylene iodonium as an inhibitor of the NADPH oxidase complex of bovine neutrophils. Factors controlling the inhibitory potency of diphenylene iodonium in a cell-free system of oxidase activation. *Eur. J. Biochem.* **208**, 61–71 (1992).
- Chen, X. et al. Apoplastic H<sub>2</sub>O<sub>2</sub> plays a critical role in axillary bud outgrowth by altering auxin and cytokinin homeostasis in tomato plants. *N. Phytol.* **211**, 1266–1278 (2016).
- Mei, Y., Chen, H., Shen, W., Shen, W. & Huang, L. Hydrogen peroxide is involved in hydrogen sulfide-induced lateral root formation in tomato seedlings. *BMC Plant Biol.* **17**, 162 (2017).
- Li, P. et al. Phase transitions in the assembly of multivalent signalling proteins. *Nature* **483**, 336–340 (2012).
- Kato, M. et al. Cell-free formation of RNA granules: low complexity sequence domains form dynamic fibers within hydrogels. *Cell* **149**, 753–767 (2012).
- Lin, Y., Protter, D. S. W., Rosen, M. K. & Parker, R. Formation and maturation of phase-separated liquid droplets by RNA-binding proteins. *Mol. Cell* **60**, 208–219 (2015).
- Jiao, C.-J. et al. β-ODAP accumulation could be related to low levels of superoxide anion and hydrogen peroxide in *Lathyrus sativus* L. *Food Chem. Toxicol.* **49**, 556–562 (2011).
- Wang, L., Wang, X. & Wang, C. Protein disulfide-isomerase, a folding catalyst and a redox-regulated chaperone. *Free Radic. Biol. Med.* **83**, 305–313 (2015).
- Lyles, M. M. & Gilbert, H. F. Catalysis of the oxidative folding of ribonuclease A by protein disulfide isomerase: dependence of the rate on the composition of the redox buffer. *Biochemistry* **30**, 613–619 (1991).
- Levy, Y. Y. & Dean, C. The transition to flowering. *Plant Cell* **10**, 1973–1989 (1998).
- Jones, D. P. Radical-free biology of oxidative stress. *Am. J. Physiol.-Cell Physiol.* **295**, C849–C868 (2008).

**Publisher's note** Springer Nature remains neutral with regard to jurisdictional claims in published maps and institutional affiliations.

© The Author(s), under exclusive licence to Springer Nature America, Inc. 2021

## Methods

**Plant materials and growth conditions.** The tomato (*Solanum lycopersicum*) cultivar M82 was used in this study. Greenhouse plants were grown under natural light with supplementation from LED (Philips Lighting IBRS, 10461, 5600 VB, NL) on a 16 h light/8 h dark photoperiod. Hydroponic seedlings were grown in a growth room at 26 °C, with 45–60% relative humidity and 12 h light/12 h dark photoperiod under 55  $\mu\text{mol m}^{-2} \text{s}^{-1}$  light intensity. For redox chemical treatment, M82 seeds were germinated on filter paper for 2 d in dark at room temperature, and the germinated seeds were transferred into soil. The seedlings at similar stages were selected and grown in hydroponic culture boxes (SJT003A, Nantong Rongcheng Agriculture) supplied by 1× Hoagland (Coolaber) medium with or without different chemical reagents. Growth and development evaluations of tomato seedlings were performed to establish the appropriate concentration of redox chemicals.

**Plasmid constructs and tomato transformation.** To make the constructs for 35S:TMF-GFP and 35S:GFP-TMF<sup>EC1125</sup>/tmf transgenic plants, the coding sequences of TMF, TMF<sup>EC1125</sup> and GFP were ligated into the pRI101 vector by In-Fusion cloning (TransGen Biotech). To produce pSuper:TMF-Myc transgenic plants, the coding sequence of TMF was directly cloned into binary vector pSuper:1300 containing the Myc tag. The resulting constructs were transformed into M82, *fa*<sup>+/+</sup> and *tmf* mutant plants by following *Agrobacterium*-mediated transformation and tissue culture protocol as described in ref. 49. To generate the constructs for transcription activity assay, the 2-kb fragment upstream of the transcription start site of AN was amplified and cloned into pCAMBIA1381-GUS vector by In-Fusion cloning. The primers are listed in Supplementary Table 1.

**Messenger RNA in situ hybridization.** mRNA in situ hybridization for TMF was conducted using standard protocols<sup>50</sup> with slight modifications. Briefly, to generate probes of TMF, a full-length coding sequence was amplified from complementary DNA using KOD Xtreme hot start DNA polymerase (Novagen), and the resulting products were ligated into StrataClone pSC-A-amp/kan vector (Agilent Technologies). Plasmids were linearized and, depending on insert orientation, T7 or T3 RNA polymerase was used for in vitro transcription (Roche). Full-length probes were used for the hybridization. For fixation, meristems were hand-dissected and fixed in 4% paraformaldehyde with 0.3% Triton-X under vacuum.

**Protein structure prediction.** IDR domains were analyzed by 'VSL2' algorithm of 'Predictor of Natural Disordered Regions' (PONOR, <http://www.pondr.com/>). DNA-binding domain of TMF was defined as previously described<sup>5</sup>.

**Recombinant protein expression and purification.** To express recombinant TMF proteins in *Escherichia coli*, the coding sequences of TMF alone and GFP-TMF fusion DNA were ligated into the pQE-80L vector by In-Fusion cloning. The resulting constructs were transformed into *E. coli* BL21 (DE3) or Rosetta (DE3) competent cells for isopropyl  $\beta$ -D-1-thiogalactopyranoside (IPTG) inducible protein expression. The *E. coli* cells were cultured in LB liquid medium at 37 °C until the optical density ( $\text{OD}_{600}$ ) went up to an optimal density (0.8–1.3) followed by cooling-down for 30 min at 4 °C, and then induced with supplementation of 0.5 mM IPTG for 16 h at 16 °C. The cells were collected by centrifugation and crushed by sonication in lysis buffer (50 mM Tris-HCl, 200 mM NaCl, pH 7.4). Cell lysates were centrifuged at 14,000g for 30 min. Protease inhibitor cocktail tablets (Roche) were added into cell lysates to protect the protein from degradation. The supernatants were initially purified by Ni-NTA (GE healthcare) affinity beads, and subsequently purified on a Superdex 200 increase 10/300 column (SD200) cascaded into an AKTA system (GE healthcare) by following the manufacturer's instructions. Benzoylase nuclease (Chejeter) and high salt buffer (50 mM Tris-HCl, 2 M KCl, pH 7.4) were used to remove prokaryotic nucleic acids from recombinantly expressed proteins. Protein ultrafiltration tubes (Vivaspin turbo) were used for protein concentration and buffer exchange. Purified proteins were examined by SDS-PAGE gels (Supplementary Fig. 1) and stored in storage buffer (50 mM Tris-HCl, 200 mM NaCl, pH 7.4) at -80 °C.

**In vitro phase separation assay.** In vitro phase separation assay was performed in buffer containing 50 mM Tris-HCl (pH 7.4) and NaCl at various concentrations as indicated in the figure legends. To remove the potentially denatured protein pellets in the bottom of tubes that might interfere experimental results, all protein samples were centrifuged at 12,000g and the resulting supernatants were transferred into new tubes before performing the phase separation assay. Protein concentrations were determined by NanoDrop spectrophotometry (IMPLEN NP80). To assess the effects of target DNA of TMF on its phase separation behavior, the 120 bp length of single-strand DNA fragments from AN promoter region were synthesized by labeling with Cy-3 (Ruibio). To produce double-strand DNAs, a touchdown PCR (Program: Final temperature (25 °C) = initial temperature (95 °C) + ((number of cycles - 1) ×  $\Delta T$  (0.1 °C s<sup>-1</sup>))) was performed to produce double-strand DNAs. The DNA concentrations were measured using NanoDrop spectrophotometry (IMPLEN NP80). The protein phase separation reacted in 1.5 ml Eppendorf tubes. Liquid droplets were observed using confocal microscopy (Leica SP5 microscope equipped with ×20 and ×40 immersion objectives). For generating

phase diagram, the samples were observed in 384-well microscopy plate (Cellvis) sealed with optically clear adhesive film. The phase diagram images were captured simultaneously under Nikon A1Rsi microscope equipped with ×60 oil immersion objective. GFP and Cy-3 fluorescence were excited at 488 or 543 nm and detected at 500–540 and 595–630 nm, respectively.

**Phase sedimentation assay.** For the sedimentation assay without DNA addition, 150  $\mu\text{M}$  His-TMF protein in the 50 mM Tris-HCl buffer with 150 mM NaCl were diluted into 25 mM NaCl to trigger phase separation. For the sedimentation assay with DNA, 150  $\mu\text{M}$  His-TMF protein and 6  $\mu\text{M}$  double-strand DNA from AN promoter region (-1,537 to -1,657 bp) were incubated with indicated concentrations of DTT and H<sub>2</sub>O<sub>2</sub> on ice for 10 min in the Tris-HCl buffer with 150 mM NaCl. The samples were then centrifuged at 20,000g for 15 min at 4 °C. The resulting supernatants were immediately transferred into new tubes and remaining pellet fractions were resuspended using Tris-HCl buffer with equal volume to the supernatants. Next 5  $\mu\text{l}$  of 20-fold diluted supernatant and pellet samples were completely reduced with 5 mM  $\beta$ -mercaptoethanol and loaded into SDS-PAGE for western blotting analysis. Anti-GFP antibody (Easybio) and horseradish peroxidase-conjugated (antirabbit) secondary antibody (Easybio) were used for protein detection. The immunoblotting signals were visualized by a chemiluminescence apparatus (Tanon 500 Multi).

**Protoplast transfection and chemical treatment.** The protoplast cells were isolated from cotyledon of tomato seedlings with two or three true leaves grown in a greenhouse under a normal growth conditions as mentioned above. Approximately 20  $\mu\text{g}$  of plasmids were transfected into protoplasts using the PEG-mediated transfection protocol as described previously<sup>51</sup>. The transfected protoplasts were incubated in W5 buffer at 22 °C in the dark. After incubation for 13 h, protoplasts were supplemented with 1 mM redox agents of H<sub>2</sub>O<sub>2</sub>, amino-1,2,4-triazole (Sigma), 5 mM KI (Macklin) and 1 mM DTT for 3 h before harvesting for microscopy observation, respectively. The Hoechst 33342 dye (5  $\mu\text{g ml}^{-1}$ ) (Invitrogen) was used to label the nuclei of protoplast cells.

**Hydrogen peroxide staining.** Fluorescence probe HPF (Alexis Biochemical) and unflorescence dye DAB (Sigma-Aldrich) were used to detect the endogenous hydrogen peroxide level in tomato SAMs. For HPF staining, the tomato young seedlings at vegetative and transition meristem stages were simply dissected to remove extra leaves and embedded in 6% agarose (VWR Chemicals). The embedded materials were then sectioned into 50- $\mu\text{m}$  thicknesses by Microtome (Leica VT1200S). The sections were incubated in the phosphate buffer (pH 6.1) containing 5  $\mu\text{M}$  HPF for 5 min. For DAB staining, meristem sections were incubated in the DAB staining buffer (1 mg ml<sup>-1</sup> DAB and 200 mM Na<sub>2</sub>HPO<sub>4</sub>, pH 6.5) for 4 h, and leaves were incubated for 12 h. The staining was then stopped in a fixing solution (ethanol:lactic acid:glycerol, 3:1:1). Images were collected using stereomicroscope (LeicaDM5000-B).

**Microscopy imaging.** Imaging for tomato protoplast cells and young leaves was performed on a Leica SP5 confocal microscope with ×20, ×40 and ×63 oil objectives. GFP was detected using 488 nm laser excitation and 500–540 nm emission filter. The Hoechst dye signals were detected with 405 nm laser excitation and a 440–480 nm emission filter. Dissection and stereomicroscope imaging of tomato meristems were carried out under Olympus microscope (SteREO Discovery, v.12) by following a standard protocol as previously reported<sup>37</sup>.

**FRAP.** FRAP of TMF-GFP condensates in transfected tomato protoplasts and transgenic plants was performed on a Zeiss 710LSM confocal microscope using a ×60 oil objective. The punctate region of TMF-GFP was bleached using a 488 nm laser pulse (65% intensity). In vitro FRAP analysis was conducted with samples in 384-well microscopy plates using a Nikon A1 microscope equipped with a ×60 oil immersion objective. Droplets with and without Cy-3 labeled DNA were bleached with a 488 nm laser pulse and 488/595 laser pulse, respectively (at least three repeats). The recovery time was recorded for the indicated time as mentioned.

**Image analysis and signal quantification.** Signal strength of the fluorescence images and immunoblotting images was quantified using ImageJ (Fiji Win64). Raw images were imported and transformed into eight-bit type. The measurements were performed according to the user guide of the software.

**Yeast one-hybrid assays.** Yeast one-hybrid assays were performed as described previously<sup>52</sup>. Briefly, the various DNA fragments from AN promoter region were cloned into pLacZi2u vector by which the *LacZ* was expressed as a reporter. The coding sequences of TMF and its mutant variants were ligated into the pB42AD vector to generate activator constructs. The resulting constructs were cotransformed into yeast strain EGY48 by following a standard yeast transformation handbook protocol (Clontech). The yeast colonies were grown on selective medium for 3 d at 28 °C. To quantify and compare the transcription regulating activity, the yeast cells were cultured in SD/-Trp-Ura liquid medium

until the OD<sub>660</sub> went up to 1.0. The cellular  $\beta$ -galactosidase activity was determined by using a yeast  $\beta$ -galactosidase assay kit (Thermo Scientific).

**ChIP-qPCR.** ChIP-qPCR assay was carried out as described previously with minor modifications<sup>53</sup>. To obtain enough vegetative meristem tissue for ChIP-qPCR assay, we transformed *TMF-Myc* fusion construct into an *fa* mutant that overproliferates vegetative meristems during inflorescence development. Young inflorescences of *pSuper:TMF-Myc/fa* transgenic plants grown in greenhouse were used for crosslinking in prechilled PBS with 1% formaldehyde (Sigma-Aldrich) buffer under vacuuming (7.5 psi). The crosslinking reaction was quenched using prechilled PBS with 0.125 M glycine solution. After washing three times with distilled deionized water, the fixed tissue was quickly ground in liquid nitrogen. The nuclei isolation and chromatin release were performed as described. The *TMF-Myc* protein was immunoprecipitated by anti-Myc antibody (Sigma) and isolated by protein A/G magnetic beads (Millipore). Data for statistical analysis were collected from three independent experiments with three technical replicates for each experiment.

**Mass spectrometric analysis of protein disulfide bonds.** Protein disulfide bond identification were performed as described before<sup>54</sup>. For the protein sample pretreatment, the purified recombinant TMF proteins were alkylated by 25 mM *N*-ethylmaleimide for 45 min at room temperature in the dark. The alkylated proteins were subjected for pepsin digestion (pepsin:protein ratio, 1:50) for 2 h at 37 °C followed by overnight trypsin digestion at 37 °C (trypsin:protein ratio, 1:50). The digested samples were loaded into Orbitrap Fusion Lumos equipped with EASY-nLC 1200 (ThermoFisher) for liquid chromatograph tandem mass spectrometry (LC-MS/MS) analysis. The resolution of MS1 and MS2 scans were set to 120,000 and 15,000, respectively. The Sol Genomics Network database ITAG3.2 was used for tomato protein sequence analysis. The search engine pLink v.2.3 (<http://pfind.ict.ac.cn/software/pLink/index.html>) was used for disulfide linkage analysis. Both precursor mass and fragment tolerance were set at 20 ppm. The *n*-ethylmaleimide [C] was set to variable modification.

**PDI assay.** The human PDI (gene accession no. AK297967) used in this study was recombinantly expressed in *E. coli* and purified as previously reported<sup>55</sup>. For the PDI assay, GFP-TMF protein was reacted with 1  $\mu$ M PDI in a classical redox balancing buffer (50 mM Tris-HCl, 150 mM NaCl, 1 mM GSH and 0.2 mM GSSG, GSH/GSSG = 5)<sup>46</sup>. For PDI catalyzed disulfide reformation, GFP-TMF protein was incubated with 100 mM DTT for 4 h to fully reduce the disulfide bonds. The DTT was then removed by dialysis using a dialysis membrane (Solarbio) and protein ultrafiltration columns (Vivaspin turbo). The dialyzed TMF proteins were incubated with 1  $\mu$ M PDI in the redox balancing buffer. All the above reactions underwent at 4 °C for 4 h before microscopy imaging.

**Transcription activity assay.** The previously reported GUS-LUC dual reporter system was used for the transcription activity analysis<sup>56</sup>. In the assays, the TMF and its cysteine mutated variant proteins served as effectors, with GFP alone as a negative control. The *GUS* gene driven by the 2-kb upstream promoter region of *AN* (*pAN:GUS*) served as a reporter. The firefly *LUC* gene driven by *CaMV* 35S promoter (*35S:LUC*) was used as an internal control. The combinations of effector and reporter plasmids were coinfiltrated into *Nicotiana benthamiana* leaves as described. After infiltration for 48 h, the leaves were treated with different chemicals, including 10 mM H<sub>2</sub>O<sub>2</sub>, 5 mM KI, 0.5 mM AT, 50  $\mu$ M SHAM (Sigma) and 0.5  $\mu$ M DPI for 12 h before harvesting. To measure the activity of GUS and luciferase (LUC) activity, the 4-methylumbelliferyl glucuronide (Sigma) and luciferin (Promega) were used as substrates, respectively. The transcriptional activity was reflected by the ratio of activity of GUS to LUC.

**Immunoblotting analysis of TMF proteins.** Total protein was extracted from young leaves of a *35S:TMF-Myc/fa* transgenic plant with lysis buffer (10 mM Tris-HCl, 150 mM NaCl, 0.5% NP40) supplemented with or without 10 mM DTT for 30 min on ice, respectively. The total proteins were loaded into SDS-PAGE for western blotting analysis. Anti-Myc antibody (Sigma) and horseradish peroxidase-conjugated (antimouse) secondary antibody (Easybio) were used for TMF-Myc protein detection, horseradish peroxidase-conjugated anti-Actin (Easybio) was used for Actin protein detection. The immunoblotting signals were visualized by a chemiluminescence apparatus (Tanon 500 Multi).

**Reporting Summary.** Further information on research design is available in the Nature Research Reporting Summary linked to

## Data availability

Source data are provided with this paper. All other data supporting the findings of this study are available within the paper and its Supplementary information files, or are available from the corresponding author upon reasonable request.

## References

- Eck, J. V., Kirk, D. D. & Walmsley, A. M. In *Agrobacterium Protocols. Methods in Molecular Biology* Vol. 343 (ed. Wang, K.) (Humana Press, 2006); <https://doi.org/10.1385/1-59745-130-4:459>
- Jackson, D. *Molecular Plant Pathology: A Practical Approach* (Oxford Univ. Press, 1992).
- Xu, C. et al. A cascade of arabinosyltransferases controls shoot meristem size in tomato. *Nat. Genet.* **47**, 784–792 (2015).
- Lin, R. et al. Transposase-derived transcription factors regulate light signaling in arabidopsis. *Science* **318**, 1302–1305 (2007).
- Gendrel, A.-V., Lippman, Z., Martienssen, R. & Colot, V. Profiling histone modification patterns in plants using genomic tiling microarrays. *Nat. Methods* **2**, 213–218 (2005).
- Shen, G. et al. Warfarin traps human vitamin K epoxide reductase in an intermediate state during electron transfer. *Nat. Struct. Mol. Biol.* **24**, 69–76 (2017).
- Li, H. et al. Crystal and solution structures of human protein-disulfide isomerase-like protein of the testis (PDILT) provide insight into its chaperone activity. *J. Biol. Chem.* **293**, 1192–1202 (2018).
- Shi, Y. et al. Ethylene signaling negatively regulates freezing tolerance by repressing expression of CBF and Type-A ARR genes in *Arabidopsis*. *Plant Cell* **24**, 2578–2595 (2012).

## Acknowledgements

We thank C.-C. Wang and L. Wang from the Institute of Biophysics, CAS for sharing PDI enzyme and valuable suggestions for related experiments, Z. B. Lippman (Cold Spring Harbor Laboratory), S. J. Park (Wonkwang University) and J. V. Eck (Boyce Thompson Institute) for sharing seeds, in situ images and the tomato transformation protocol, respectively. We thank J. Y. Li, Z. B. Lippman, J. Yang, K. Jiang and Q. Y. Wu for valuable comments and discussions; S. H. Yang and J. G. Li for sharing transformation vectors; Y. B. Tian, L. Fu, Z. Lu and S. Q. Jia for technical support and Y. F. Chen, W. X. Dong, Q. L. Guo, Y. Yu, Y. Xie, T. H. Zhang and X. Tong in the Xu laboratory for their help in this study. We are grateful to the staff from facilities of State Key Laboratory of Plant Genomics, Institute of Genetics and Developmental Biology, CAS; Institute of Botany, CAS and Tsinghua University for technical assistance. This study was financially supported by the Key Research Program of Frontier Sciences of the Chinese Academy of Science (grant no. ZDBS-LY-SM021) and the Strategic Priority Research Program of Chinese Academy of Sciences (grant no. XDA24030503) to C.X., a National Key R&D grant (no. 2019YFA0508403) and a NSFC grant (no. 31871443) to P.L. and start-up funding from State Key Laboratory of Plant Genomics and Institute of Genetics and Developmental Biology to C.X. and a NSFC grant (no. 31900174) to X.H.

## Author contributions

C.X. and P.L. designed the research. X.H. performed in vivo condensate assays, chemical treatments, gene expression, immunoblots, ChIP-qPCR and transcriptional activity assays with help from N.X., S.C. and W. Li performed in vitro phase separation assays. S.C. performed EMSA, protein sedimentation assays and PDI treatments. X.H. and N.X. produced CRISPR mutants and transgenic lines with the help from X.Z. L.T. performed the yeast one-hybrid assay. Y. Zhang and W. Liu performed in situ hybridization and H<sub>2</sub>O<sub>2</sub> staining. N.Y. performed mass spectrometric analysis. Y. Zou performed bioinformatic analysis. C.X. and P.L. wrote the paper with input from all other authors.

## Competing interests

The authors declare no competing interests.

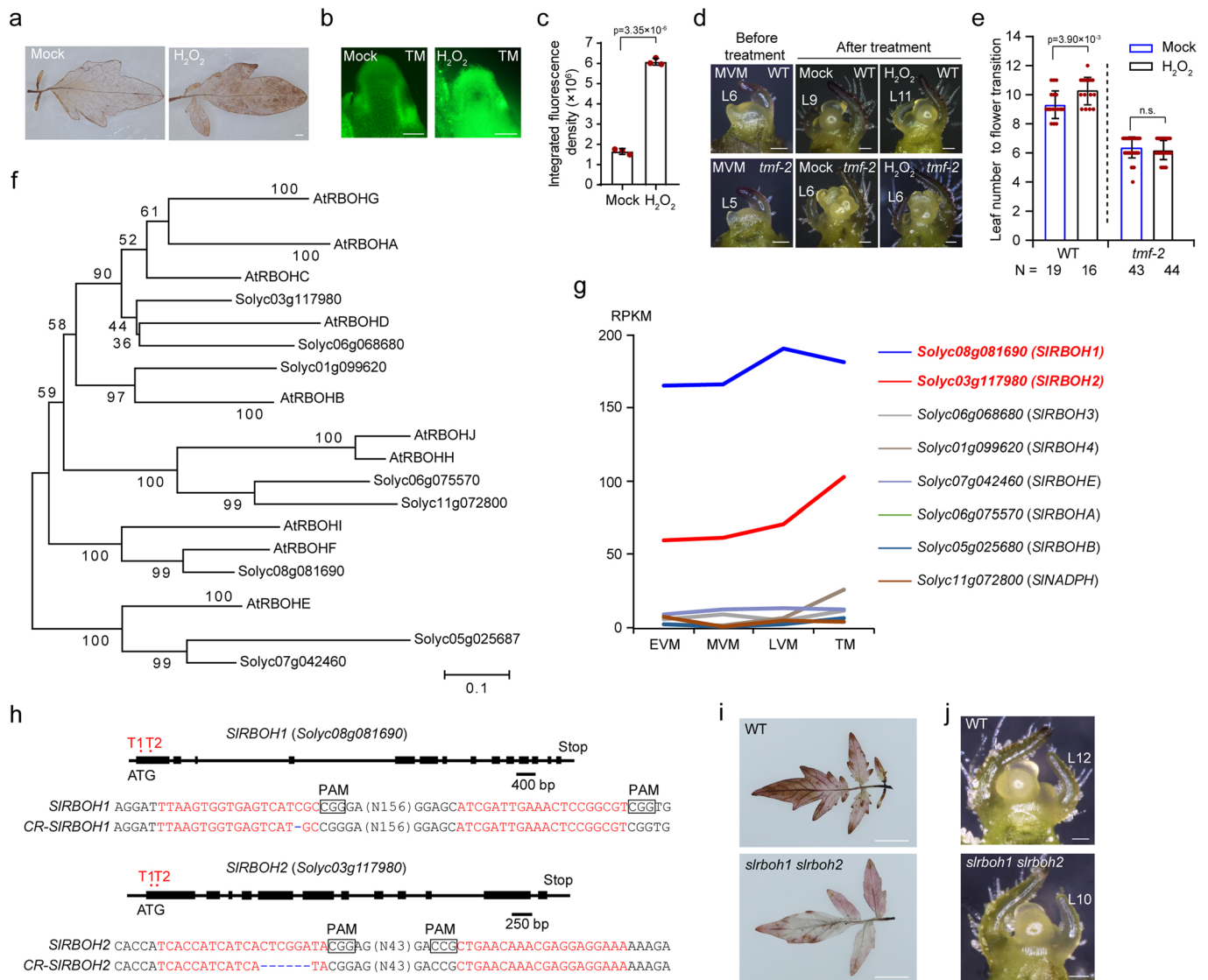
## Additional information

Extended data is available for this paper at <https://doi.org/10.1038/s41589-021-00739-0>.

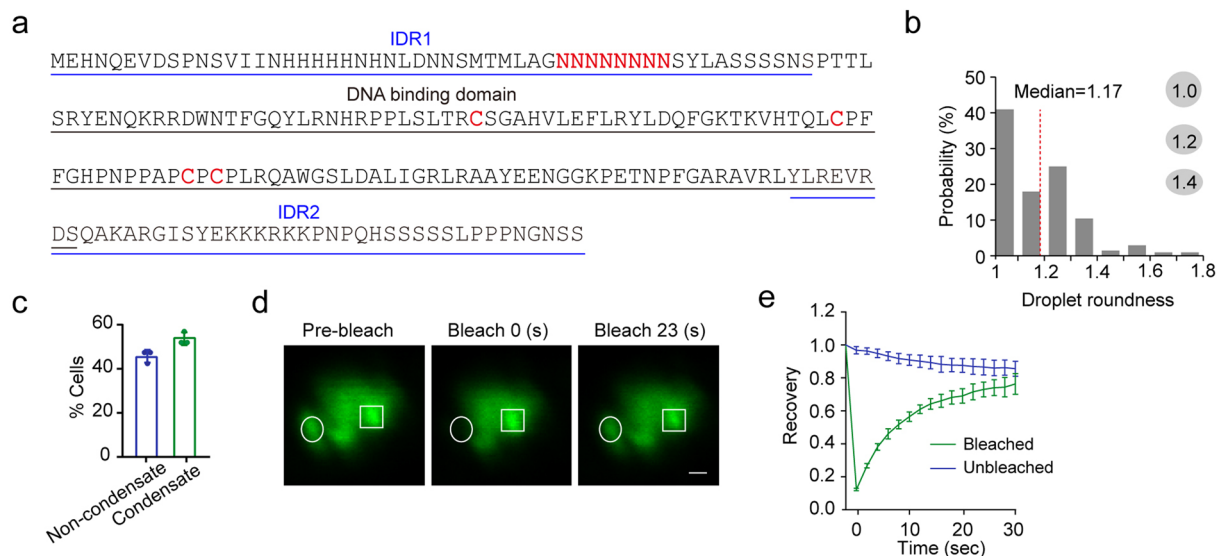
Supplementary information The online version contains supplementary material available at <https://doi.org/10.1038/s41589-021-00739-0>.

Correspondence and requests for materials should be addressed to P.L. or C.X.

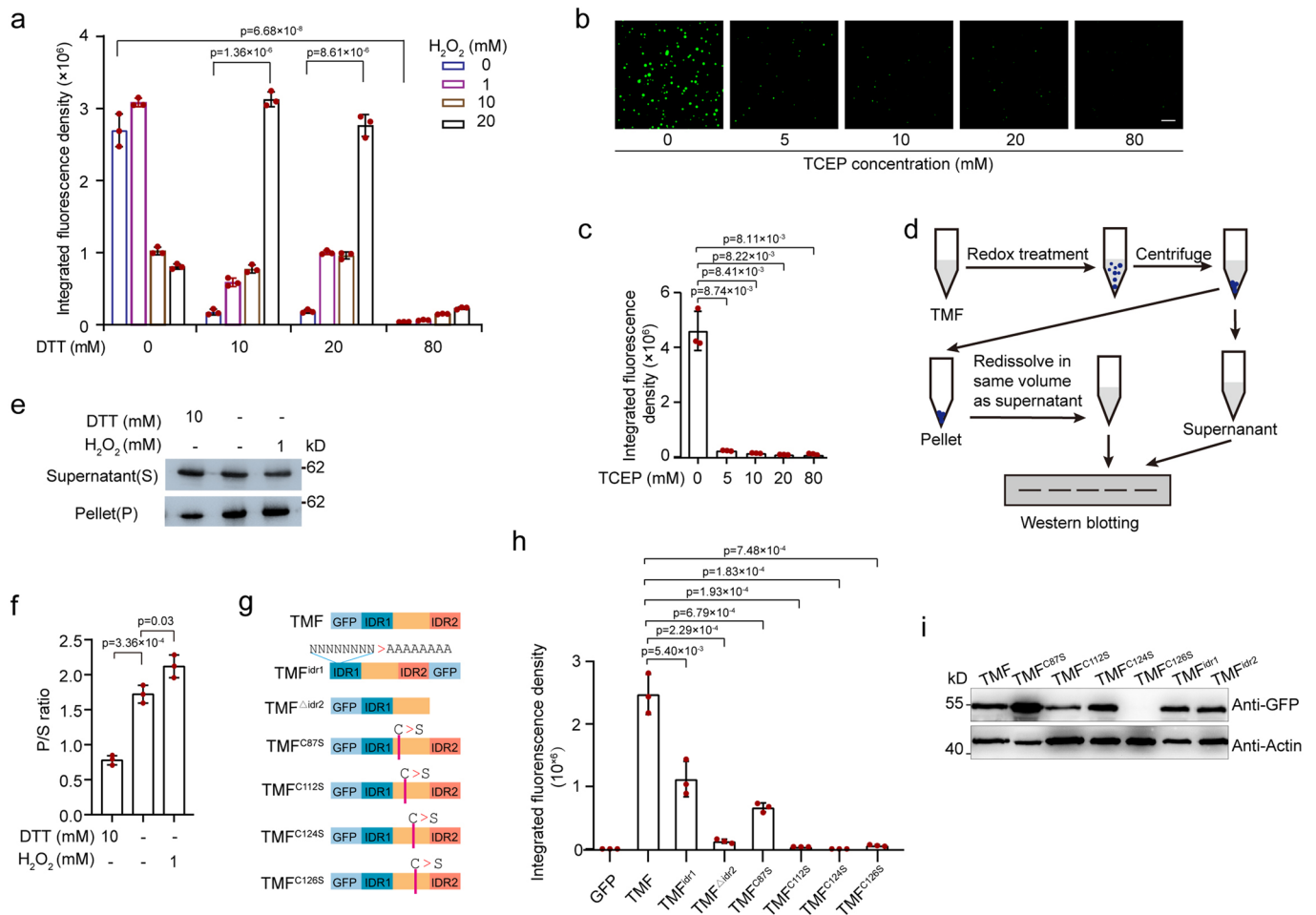
Reprints and permissions information is available at [www.nature.com/reprints](http://www.nature.com/reprints).



**Extended Data Fig. 1 | Images and quantification data for hydrogen peroxide staining and redox chemical treatments. a**, DAB staining and stereoscope imaging showing the accumulation of  $H_2O_2$  in tomato young leaves treated with or without  $H_2O_2$  (10 mM) for 36 h. **b,c**, HPF staining (**b**) and quantitative data (**c**) showing the accumulation of  $H_2O_2$  in the meristem treated with or without  $H_2O_2$  (10 mM) for 48 h. ( $n=3$ ). **d,e**, Stereoscope images (**d**) and quantitative data (**e**) comparing flowering transition indicated by leaf production until floral meristem stage transition from mock and  $H_2O_2$  (10 mM) treated WT (upper) and *tmf-2* (bottom). Leaf production is indicated by leaf number. L, Leaf. Scale bar, 100  $\mu$ m. Data are presented as means ( $\pm$  s.d.). Sample size used for statistics of mock and  $H_2O_2$  treatment for WT and *tmf-2* is 19, 16, 43, 44, respectively. **f**, Phylogeny tree showing RBOH gene family in tomato. **g**, Expression of SIRBOH genes during meristem maturation of tomato. **h**, CRISPR/Cas9 gRNAs for targeting SIRBOH genes. **i**, DAB staining showing decreased  $H_2O_2$  level in CRISPR mutant of *slrbh1 slrbh2*. Scale bar, 0.9 cm. **j**, Stereoscope images comparing flowering transition indicated by leaf production until floral meristem stage transition from WT and *slrbh1 slrbh2* mutant, L, leaf. Scale bar, 100  $\mu$ m. Three independent assays with similar results were carried out. In **c** and **e**, data are presented as means ( $\pm$  s.d.)(two-tailed t-test).

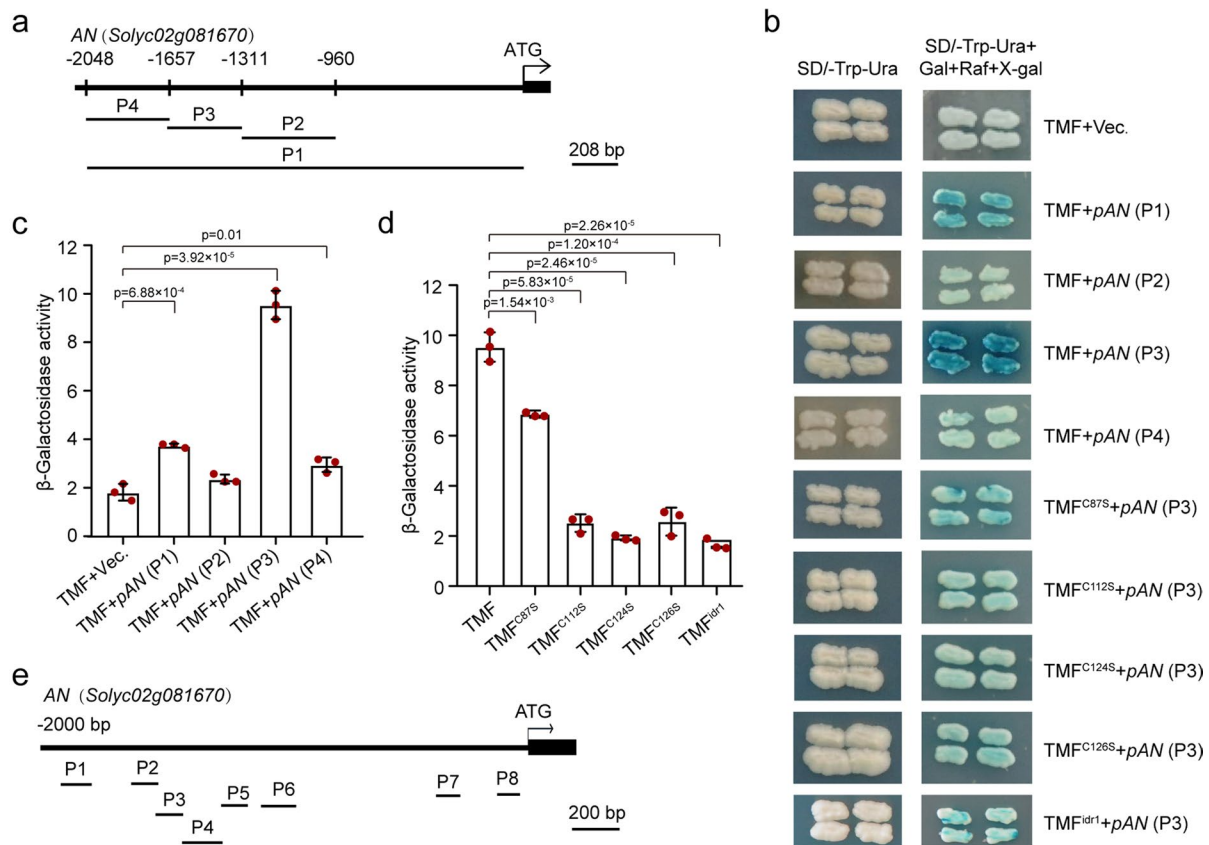


**Extended Data Fig. 2 | Droplet property and FRAP analysis of TMF-GFP condensates.** **a**, Amino acid sequence of TMF indicating IDRs, putative DNA binding domain and cysteine residues. **b**, Aspect ratios (maximal diameter/ minimal diameter) of droplets formed GFP-TMF. Gray ellipses show a guide to the eye of different aspect ratios. Totally, 202 droplets were measured for aspect ratio calculation. **c**, Quantification of TMF-GFP transfected tomato protoplast cells with or without condensates in nuclei. Three independent experiments were performed for quantification. Data are presented as ( $\pm$  s.d.) ( $n = 48$ ). **d,e**, Image (**d**) and quantitative data (**e**) showing the recovery of TMF-GFP condensates after photobleaching in tomato protoplasts. The bleached (green line) event occurs at time = 0 s. The unbleached (blue line) was used as control. Quantitative data are representative of three independent photobleaching events. Data are presented as ( $\pm$  s.d.) ( $n = 3$ ).

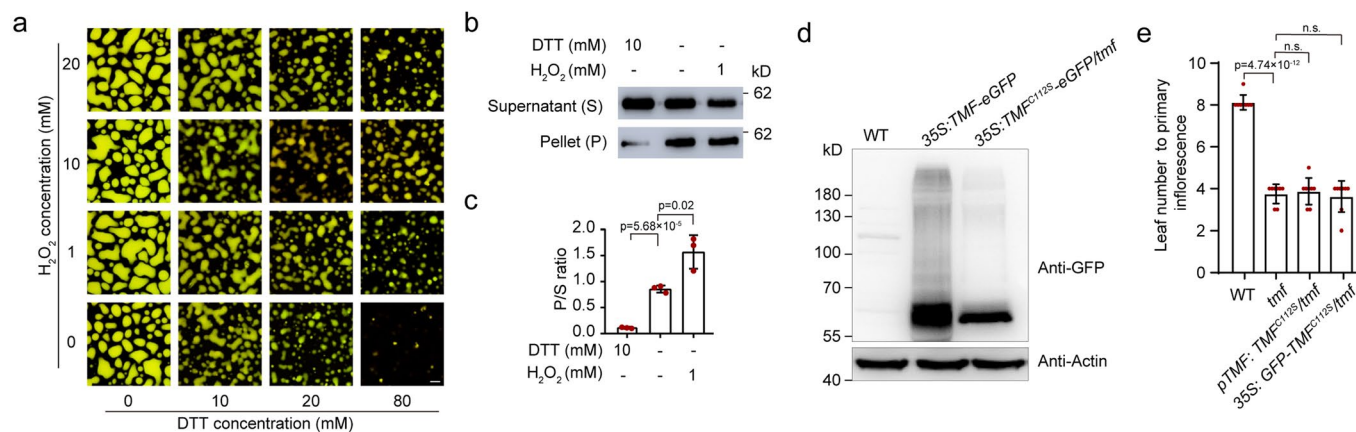


**Extended Data Fig. 3 | Quantification data and representative images for protein behavior of TMF and its mutated variants after redox chemicals treatment.** **a**, Quantification of integrated fluorescence density of the liquid-like droplets formed by GFP-TMF protein under various concentration combinations of H<sub>2</sub>O<sub>2</sub> and DTT with constant protein concentration (25 μM). **b, c**, Representative confocal images (**b**) and quantification data (**c**) showing effects of TCEP treatment on droplet formation of GFP-TMF proteins. Protein concentration, 20 μM; Salt concentration, 25 mM. Scale bar, 20 μm. **d**, Schematic sedimentation assay for redox regulated phase separation. **e, f**, Immunoblotting (**e**) and quantification data (**f**) showing the distribution of TMF proteins between aqueous-solution/supernatant (S) and condensed liquid phase/pellet (P) fractions after H<sub>2</sub>O<sub>2</sub> or DTT treatments. **g**, Schematics showing TMF variants with IDR or cysteine mutations. **h**, Quantification of integrated fluorescence density of the droplets formed by TMF variants with IDR or cysteine mutations. **i**, Immunoblot analysis showing the expression for TMF and variants with IDR or cysteine mutations in tomato protoplast. Actin serves as a loading control. In **a, c, f, h**, three technical replicates data are presented as means (± s.d.) (n = 3, two-tailed *t*-test).





**Extended Data Fig. 5 | Representative colonies and quantification data of yeast one-hybrid assay.** **a**, Promoter regions upstream of the *AN* gene selected for yeast one hybrid assays in (b-d). **b-d**, Colony growth assessment (**b**) and quantification of  $\beta$ -galactosidase activity (**c,d**) in yeast one-hybrid assay. **e**, Promoter regions upstream of the *AN* gene selected for evaluating the ChIP enrichments. In **c** and **d**, three biological replicates data are presented as means ( $\pm$  s.d.) ( $n = 3$ , two-tailed *t*-test).



**Extended Data Fig. 6 | Quantification data for droplets, phase sedimentation assay and leaf production for flower transition.** **a**, Phase diagram showing droplets formed by GFP-TMF protein and Cy-3 labeled DNA fragments under various concentration combinations of H<sub>2</sub>O<sub>2</sub> and DTT with constant protein concentration. Scale bar, 5  $\mu$ m. **b,c**, Immunoblotting (**b**) and quantification data (**c**) showing the distribution of TMF-DNA complex between aqueous-solution/supernatant (S) and condensed liquid phase/pellet (P) fractions after H<sub>2</sub>O<sub>2</sub> or DTT treatments. Three technical replicates data are presented. **d**, Western blot analysis showing expression of proteins in transgenic plants. The Wild-type (WT) plant sample served as a negative control, actin served as a loading control. **e**, Quantification of leaf number to flower transition on primary shoots. In **c** and **e**, data are means ( $\pm$  s.d.) ( $n = 3$  for **c**,  $n = 8$  for **e**, two-tailed  $t$ -test).

## Reporting Summary

Nature Research wishes to improve the reproducibility of the work that we publish. This form provides structure for consistency and transparency in reporting. For further information on Nature Research policies, see [Authors & Referees](#) and the [Editorial Policy Checklist](#).

### Statistics

For all statistical analyses, confirm that the following items are present in the figure legend, table legend, main text, or Methods section.

n/a Confirmed

- |                                     |                                     |  |
|-------------------------------------|-------------------------------------|--|
| <input type="checkbox"/>            | <input checked="" type="checkbox"/> | The exact sample size ( $n$ ) for each experimental group/condition, given as a discrete number and unit of measurement  |
| <input type="checkbox"/>            | <input checked="" type="checkbox"/> | A statement on whether measurements were taken from distinct samples or whether the same sample was measured repeatedly  |
| <input type="checkbox"/>            | <input checked="" type="checkbox"/> | The statistical test(s) used AND whether they are one- or two-sided<br><i>Only common tests should be described solely by name; describe more complex techniques in the Methods section.</i>   |
| <input checked="" type="checkbox"/> | <input type="checkbox"/>            | A description of all covariates tested   |
| <input checked="" type="checkbox"/> | <input type="checkbox"/>            | A description of any assumptions or corrections, such as tests of normality and adjustment for multiple comparisons  |
| <input type="checkbox"/>            | <input checked="" type="checkbox"/> | A full description of the statistical parameters including central tendency (e.g. means) or other basic estimates (e.g. regression coefficient) AND variation (e.g. standard deviation) or associated estimates of uncertainty (e.g. confidence intervals) |
| <input type="checkbox"/>            | <input checked="" type="checkbox"/> | For null hypothesis testing, the test statistic (e.g. $F$ , $t$ , $r$ ) with confidence intervals, effect sizes, degrees of freedom and $P$ value noted<br><i>Give <math>P</math> values as exact values whenever suitable.</i>                            |
| <input checked="" type="checkbox"/> | <input type="checkbox"/>            | For Bayesian analysis, information on the choice of priors and Markov chain Monte Carlo settings   |
| <input checked="" type="checkbox"/> | <input type="checkbox"/>            | For hierarchical and complex designs, identification of the appropriate level for tests and full reporting of outcomes   |
| <input checked="" type="checkbox"/> | <input type="checkbox"/>            | Estimates of effect sizes (e.g. Cohen's $d$ , Pearson's $r$ ), indicating how they were calculated   |

*Our web collection on [statistics for biologists](#) contains articles on many of the points above.*

### Software and code

Policy information about [availability of computer code](#)

Data collection Data collection was performed manually and captured using Microsoft Excel 2013

Data analysis Statistical analyses were performed using Microsoft Excel 2013, R 3.5.1, Sigmaplot 10.0. Significances of difference were analyzed by two-tailed t-test. In all cases,  $n$  is as indicated;  $p$  is defined as follows: \*,  $p < 0.05$ ; \*\*,  $p < 0.01$ ; \*\*\*,  $p < 0.001$ .

For manuscripts utilizing custom algorithms or software that are central to the research but not yet described in published literature, software must be made available to editors/reviewers. We strongly encourage code deposition in a community repository (e.g. GitHub). See the Nature Research [guidelines for submitting code & software](#) for further information.

### Data

Policy information about [availability of data](#)

All manuscripts must include a [data availability statement](#). This statement should provide the following information, where applicable:

- Accession codes, unique identifiers, or web links for publicly available datasets
- A list of figures that have associated raw data
- A description of any restrictions on data availability

Figures 1-5, Extended Data Figures 1-6. No restrictions on data availability. All data used as part of this study are included in this manuscript or its Extended Data and Supplementary Materials or are available upon request from the corresponding author.

## Field-specific reporting

Please select the one below that is the best fit for your research. If you are not sure, read the appropriate sections before making your selection.

Life sciences       Behavioural & social sciences       Ecological, evolutionary & environmental sciences

For a reference copy of the document with all sections, see [nature.com/documents/nr-reporting-summary-flat.pdf](https://www.nature.com/documents/nr-reporting-summary-flat.pdf)

## Life sciences study design

All studies must disclose on these points even when the disclosure is negative.

Sample size	Given that all genotypes analyzed were either wild type controls or stable homozygous mutants, > 10 biological replicates for meristems were analyzed in each experiment for data presented in this study. For statistical analysis, two-tailed t-test was used.
Data exclusions	No data excluded.
Replication	All presented either in Methods or Supplementary information.
Randomization	Seedlings used for phenotyping were grown side by side with several replicates, and multiple times at greenhouse.
Blinding	Not applicable.

## Reporting for specific materials, systems and methods

We require information from authors about some types of materials, experimental systems and methods used in many studies. Here, indicate whether each material, system or method listed is relevant to your study. If you are not sure if a list item applies to your research, read the appropriate section before selecting a response.

### Materials & experimental systems

n/a	Involvement in the study
<input type="checkbox"/>	<input checked="" type="checkbox"/> Antibodies
<input checked="" type="checkbox"/>	<input type="checkbox"/> Eukaryotic cell lines
<input checked="" type="checkbox"/>	<input type="checkbox"/> Palaeontology
<input checked="" type="checkbox"/>	<input type="checkbox"/> Animals and other organisms
<input checked="" type="checkbox"/>	<input type="checkbox"/> Human research participants
<input checked="" type="checkbox"/>	<input type="checkbox"/> Clinical data

### Methods

n/a	Involvement in the study
<input checked="" type="checkbox"/>	<input type="checkbox"/> ChIP-seq
<input checked="" type="checkbox"/>	<input type="checkbox"/> Flow cytometry
<input checked="" type="checkbox"/>	<input type="checkbox"/> MRI-based neuroimaging

## Antibodies

Antibodies used	Monoclonal antibodies (Anti-His) against TMF-His was sourced from BPI. Goat anti-mouse IgG HRP-conjugated secondary antibodies was purchased from EasyBio.
Validation	Validation of commercially available antibodies is provided by the supplier.